Biomedicine & Pharmacotherapy 195 (2026) 119051

Contents lists available at ScienceDirect

Biomedicine & Pharmacotherapy

journal homepage: www.elsevier.com/locate/biopha

Astaxanthin improves behavioural and immune dysfunction in the *Shank3b* mouse model of autism spectrum disorder

Anjana Madhavan [a,1], Martina Schiano-Visconte [a], Lauren Dutton [a], Mattia Cantalupo [a], Luigi Balasco [a,b], Alessia Mavillonio [a,2], Gabriele Chelini [a,c], Yuri Bozzi [a,c], Luca Pangrazzi [a,d,*]

[a] CIMeC - Center for Mind/Brain Sciences, University of Trento, Piazza della Manifattura 1, Rovereto, Trento 38068, Italy
[b] Department of Life Sciences and Public Health, Università Cattolica del Sacro Cuore, Rome 00168, Italy
[c] CNR Neuroscience Institute, Pisa 56124, Italy
[d] Institute for Biomedical Aging Research, Universität Innsbruck, Rennweg 10, Innsbruck 6020, Austria

ARTICLE INFO

Keywords:
Autism
ASD
Inflammation
Cerebellum
Microglia

ABSTRACT

Autism spectrum disorder (ASD) is a neurodevelopmental condition characterized by deficits in social communication and interaction, and repetitive behaviours. Numerous studies have associated ASD with immune dysregulation and inflammation, with neuroinflammatory processes reported in ASD individuals and mouse models. Altered immune cell profiles and cytokine levels have been observed in the peripheral blood (PB), supporting systemic immune dysfunction. Recently we showed that the administration of antioxidant molecule N-acetylcysteine (NAC) reduced oxidative stress and inflammation and counteracted behavioural deficits in two mouse models of ASD, providing a rationale for exploring other redox-active compounds. Here, we investigated the effects of astaxanthin (AST), potent antioxidant and anti-inflammatory molecule, in the Shank3b model (*Shank3b*$^{-/-}$ mice). AST treatment significantly improved core ASD-like behaviours, including social interaction deficits, motor incoordination, and repetitive grooming. In the cerebellum, AST reduced pro-inflammatory cytokines and counteracted microglial hyperactivation. In peripheral immune compartments, AST modulated cytokine expression. Pro-inflammatory markers were downregulated in *Shank3b*$^{-/-}$ mice in the bone marrow and spleen while they were elevated in Shank3b controls, suggesting immune rebalancing (*i.e.* adaptive modulation suppressing harmful inflammation while supporting protective immunity). As a limitation, oxidative stress assays were not performed here. Receiver operating characteristic (ROC) analysis suggests that TNF and IFNγ expression in peripheral immune cells may be promising biomarkers of treatment response. Notably, unlike NAC, AST did not induce pro-inflammatory effects in *Shank3b*$^{+/+}$ animals. These findings show that AST administration may counteract behavioural deficits and immune dysfunction in *Shank3b*$^{-/-}$ mice, therefore suggesting its potential as a safe immunomodulatory therapy for ASD.

1. Introduction

Autism Spectrum Disorder (ASD) represents a group of neurodevelopmental conditions defined by deficits in social communication and restrictive, repetitive behaviours [1]. In addition to the two core behavioural impairments, individuals frequently experience a range of associated symptoms including motor impairments, coordination difficulties, epilepsy, anxiety, depression, obsessive-compulsive disorder (OCD), and attention-deficit/hyperactivity disorder (ADHD, [2]). Epidemiological studies suggest that around one in every hundred children worldwide is diagnosed with ASD, although reported prevalence can be higher in certain populations [3,4]. The etiopathogenesis of ASD is multifactorial, shaped by interactions between genetic risk factors and environmental influences throughout development [5]. Over

* Corresponding author at: Institute for Biomedical Aging Research, Universität Innsbruck, Rennweg 10, Innsbruck 6020, Austria.
E-mail address: luca.pangrazzi@uibk.ac.at (L. Pangrazzi).
[1] Current address: Laboratory of Molecular and Behavioural Neuroscience, Institute for Neuroscience, Department of Health Sciences and Technology, ETH Zurich, Switzerland
[2] Current address: Department of Cellular, Computational, and Integrative Biology (CIBIO), University of Trento, via Sommarive 9, 38123 Trento, Italy

https://doi.org/10.1016/j.biopha.2026.119051
Received 10 October 2025; Received in revised form 9 January 2026; Accepted 21 January 2026
Available online 23 January 2026

the past two decades, large-scale studies have catalogued numerous ASD risk genes and proposed some intervention approaches. Nonetheless, clinically effective treatments for the core and associated symptoms of ASD remain elusive.

Growing evidence implicates immune dysregulation and chronic inflammation as central features in ASD [6,7]. Indeed, ASD individuals are known to display altered immune cell populations, abnormal cytokine profiles, and increased expression of pro-inflammatory molecules including interleukin-6 (IL-6), tumor necrosis factor (TNF), interleukin-1β (IL-1β), and interferon-γ (IFN-γ) both in peripheral blood (PB) and in the brain [8,9]. *Post-mortem* and imaging studies consistently reveal microglial activation and neuroinflammatory changes in ASD brains [10]. These findings link immune cell over-activation to neuronal and behavioural disruptions. In parallel oxidative stress, characterized by excessive production of reactive oxygen species (ROS) and a decrease in antioxidant capacity, is frequently observed in ASD patients as well as in mouse models [6, 11–14]. Redox imbalance further exacerbates neuroimmune disturbances, perpetuating inflammation and cellular injury within neural circuits that regulate social, cognitive, and motor functions. Thus, genetic and environmental risk factors synergistically promote redox and immune aberrations, establishing a vicious cycle between the accumulation of ROS and neuroinflammation. For this reason, oxidative stress and inflammation are increasingly considered therapeutic targets for ASD intervention [11,15,16].

Mice lacking the SH3 and multiple ankyrin repeat domains protein 3b (*Shank3b*$^{-/-}$ mice) have been proposed as a valuable mouse model to study ASD, as they exhibit deficits in social interaction, impaired locomotor activity, and repetitive self-injurious grooming [17,18]. In humans, mutations in the SHANK3 gene have been associated with the development of 22q13 deletion syndrome (Phelan-McDermid Syndrome) and other non-syndromic forms of ASD [19]. Our recent work on two mouse models of ASD (*Shank3b*$^{-/-}$ mice and mice lacking contactin-associated protein 2, *Cntnap2*$^{-/-}$ mice) identified oxidative stress and proinflammatory dysfunction in the cerebellum and in peripheral organs of mutant mice [20–22]. In both models, pro-inflammatory impairments and some ASD-related behaviours could be counteracted by the chronic administration of the antioxidant/anti-inflammatory molecule N-acetylcysteine (NAC; 20, 21). Despite this, the clinical application of NAC may be limited by side effects in control animals, including a mild increase in oxidative stress and pro-inflammatory molecules in the cerebellum, emphasizing the need for alternative treatments with better safety profiles [20].

In this study, we evaluated the effects of oral astaxanthin (AST) administration on behavioural, neuroinflammatory, and immune parameters in *Shank3b*$^{-/-}$ and *Shank3b*$^{+/+}$ mice. AST is a naturally occurring xanthophyll carotenoid, known for its potent anti-inflammatory and antioxidant properties [23,24]. It is predominantly produced by microalgae such as *Haematococcus pluvialis*, as well as by yeast species like *Xanthophyllomyces dendrorhous*, and accumulates in various aquatic animals including salmon, trout, krill, shrimp, and crayfish. AST has demonstrated neuroprotective effects in several neurological disorders, including Alzheimer's disease, Parkinson's disease, and multiple sclerosis, where it helps to mitigate oxidative stress, reduce neuroinflammation, and improve neuronal survival and function [23]. However, its therapeutic potential in ASD has been poorly investigated.

Our work described that AST treatment in *Shank3b*$^{-/-}$ mice significantly improved core ASD-related behaviours, including social interaction, motor coordination, and repetitive grooming. Additionally, AST broadly decreased the expression of pro-inflammatory cytokines and chemokines while counteracting microglial hyperactivation in the cerebellum, indicating a reduction in neuroinflammation. In parallel, improved immune functions were observed in the bone marrow (BM), spleen, and PB. Taken together, these findings suggest that AST may represent a promising therapeutic option to alleviate ASD-associated behavioural and immune dysfunctions, showing enhanced efficacy to NAC by producing broader behavioural improvements, while avoiding pro-oxidant effects and the upregulation of pro-inflammatory molecules in wild-type mice.

2. Results

2.1. Astaxanthin treatment improves ASD-related behaviours in *Shank3b*$^{-/-}$ mice

Administration of antioxidant and anti-inflammatory compounds has been shown to modulate behavioural impairments in ASD mouse models, including *Shank3b*$^{-/-}$ mice [21]. To further investigate this, we tested the impact of AST treatment on social, motor, and repetitive behaviours in *Shank3b*$^{-/-}$ and *Shank3*$^{+/+}$ mice administered AST or vehicle (oil, control; Fig. 1). *Shank3*$^{+/+}$ mice consistently preferred the social chamber (SC) in the three-chamber social interaction test, regardless of treatment. In contrast, control *Shank3b*$^{-/-}$ mice spent comparable amounts of time in the social and empty chambers (EC; Fig. 1a). Remarkably, AST-treated *Shank3b*$^{-/-}$ mice showed increased preference for the SC. Correspondingly, AST administration restored the social index of *Shank3b*$^{-/-}$ mice to levels comparable to those observed in the *Shank3*$^{+/+}$ groups. Motor coordination was assessed using the rotarod test (Fig. 1b). *Shank3b*$^{-/-}$ control mice spent significantly less time on the rotarod compared to *Shank3*$^{+/+}$ oil-treated mice. However, AST-treated *Shank3b*$^{-/-}$ animals showed improved rotarod performance, spending as much time on the apparatus as the *Shank3*$^{+/+}$ counterpart. Assessment of repetitive behaviours (grooming) revealed that AST treatment reduced grooming frequency in *Shank3b*$^{-/-}$ animals (Fig. 1c). No significant effects were observed following AST treatment in the open field test (Figure S1). Collectively, these findings indicate that AST administration can ameliorate key ASD-related behavioural deficits in *Shank3b*$^{-/-}$ mice.

2.2. Astaxanthin reduces molecules related to inflammation and counteracts microglia hyperactivation in the cerebellum of *Shank3b*$^{-/-}$ and *Shank3b*$^{+/+}$ mice

We next examined whether AST could mitigate the pro-inflammatory environment in the cerebellum of *Shank3b*$^{-/-}$ mice (Fig. 2). To this end, we performed a comprehensive analysis of canonical pro-inflammatory mediators at both the mRNA and protein levels after administering AST or vehicle (Fig. 2a). In cells stimulated with PMA, ionomycin, and brefeldin A, IL-1β protein levels were reduced following AST treatment in mutant mice, while IL-1β mRNA was also decreased in *Shank3b*$^{+/+}$ animals (Fig. 2b). Similarly, TNF expression was reduced at both mRNA and protein levels in *Shank3b*$^{-/-}$ mice after AST administration, with lower mRNA levels also observed in *Shank3b*$^{+/+}$ mice (Fig. 2c). A parallel downregulation was seen for a panel of additional neuroinflammatory and chemotactic molecules (IL-6, IFNγ, CCL2, CCL3), and a group of matrix metalloproteinases (MMP3, MMP8, MMP12), well-established contributors to neuroimmune activation and strongly implicated in ASD-related neuroinflammation [7,25]. In nearly all cases, the levels of these molecules were lower in both mutant and *Shank3b*$^{+/+}$ mice following AST administration (Fig. 2d–j). No differences in the expression of GSR, SOD1 and SOD2 were observed (Fig. 2k-m). These results suggest that AST broadly reduces pro-inflammatory mediators in the cerebellum.

Microglial activation and morphological conversion towards hypertrophied, hyper-ramified phenotypes are known to correlate with both behavioural dysfunctions and local inflammation in cerebellar circuits [26]. We therefore assessed microglial phenotype in the Crus 1 cerebellar region (Fig. 3). Representative pictures of microglia cells in all conditions are shown in Fig. 3a. Quantification of iba-1^{+} cells revealed no difference between control *Shank3b*$^{-/-}$ and *Shank3b*$^{+/+}$ mice (Fig. 3b). However, AST treatment reduced microglial numbers in both groups. Morphologically, microglia from oil-treated *Shank3b*$^{-/-}$ animals were hyper-ramified, consistent with an activated state. In contrast, this

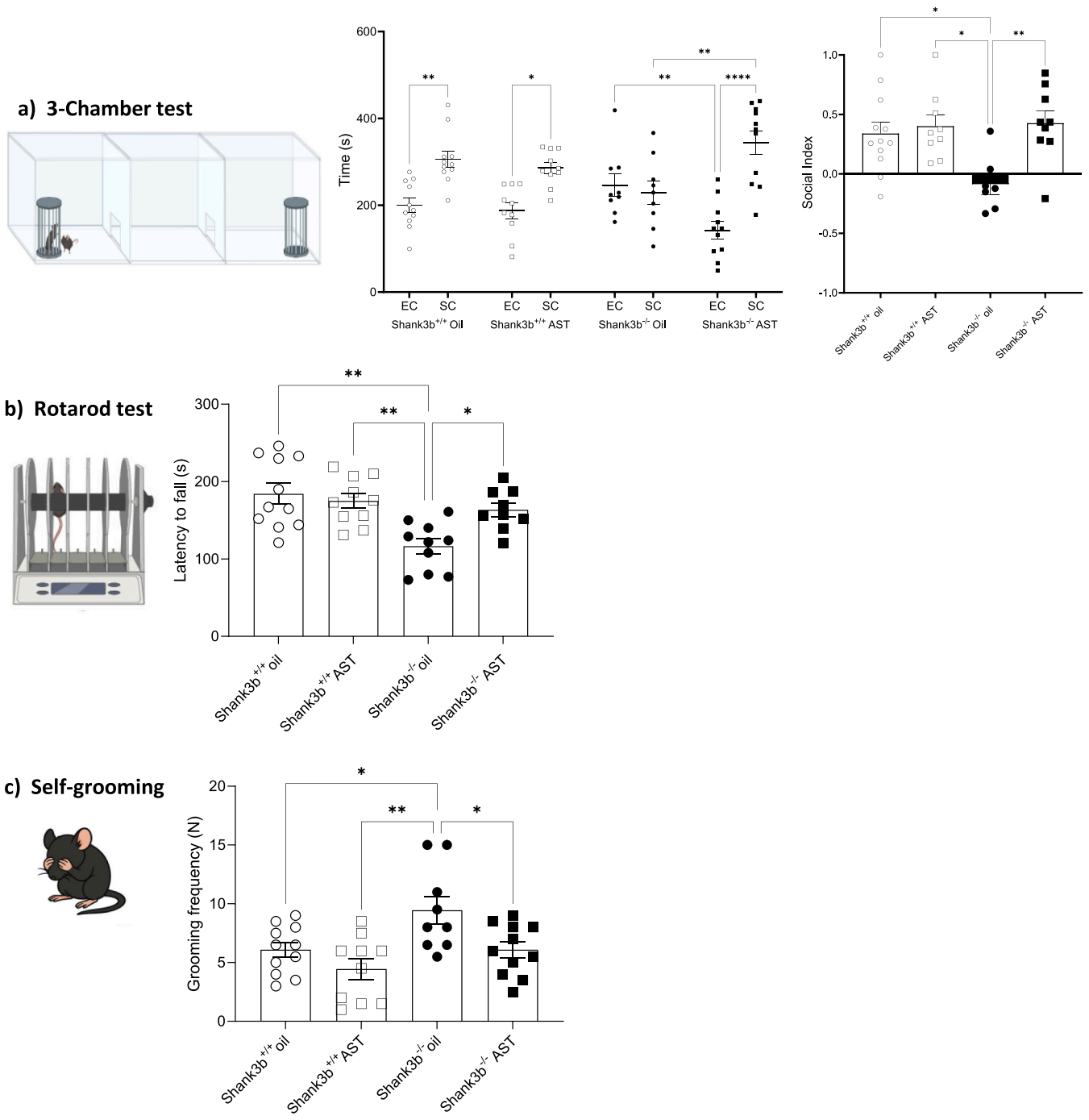

Fig. 1. Behavioural tests in in *Shank3b*$^{-/-}$ and *Shank3b*$^{+/+}$ mice treated with astaxanthin (AST). (**a**) Time spent in the empty chamber (EC) and in the social chamber (SC) in the 3-Chamber social test and sociability index (time in the sniffing zone of mouse chamber – time in the sniffing zone of empty chamber)/ total time in the sniffing zones) in AST-treated *Shank3b*$^{+/+}$ and *Shank3b*$^{-/-}$ mice and vehicle-treated control animals. (**b**) Time on rotarod (latency to fall, s) in the rotarod test. **(c)** Grooming frequency (N) in the self-grooming test. n = 11 (*Shank3b*$^{+/+}$, oil), n = 10 (*Shank3b*$^{+/+}$, AST), n = 9–10 (*Shank3b*$^{-/-}$, oil), n = 10–11 (*Shank3b*$^{-/-}$, AST). Two-way ANOVA, Tukey post-hoc test. *p < 0.05; **p < 0.01, ****p < 0.0001. Data are expressed as Mean ± SD.

phenotype was reversed after AST administration, with microglial morphology restored to levels comparable to *Shank3b*$^{+/+}$ controls (Fig. 3c). We further examined microglial activation using the markers CD11b and Ly6c (Fig. 3d,e). Interestingly, both molecules were diminished in AST-treated *Shank3b*$^{-/-}$ mice, suggesting reduced inflammation-mediated microglial activation. These findings collectively suggest that, by reducing cerebellar inflammation, AST subsequently counteracts the hyper-ramified morphology and over-activated microglia in *Shank3b*$^{-/-}$ mice.

2.3. Astaxanthin reduces molecules related to inflammation in the bone marrow of Shank3b$^{-/-}$ *and Shank3b*$^{+/+}$ *animals*

We previously documented a imbalance in the production of pro-inflammatory molecules in the peripheral organs of *Shank3b*$^{-/-}$ mice [21,22]. Therefore, we investigated whether AST administration could normalize the expression of pro-inflammatory markers in the BM of Shank3b mutant and control mice (Fig. 4). IL-1β mRNA expression was significantly reduced in *Shank3b*$^{+/+}$ animals compared with oil-treated controls, whereas no significant changes were observed in mutant mice

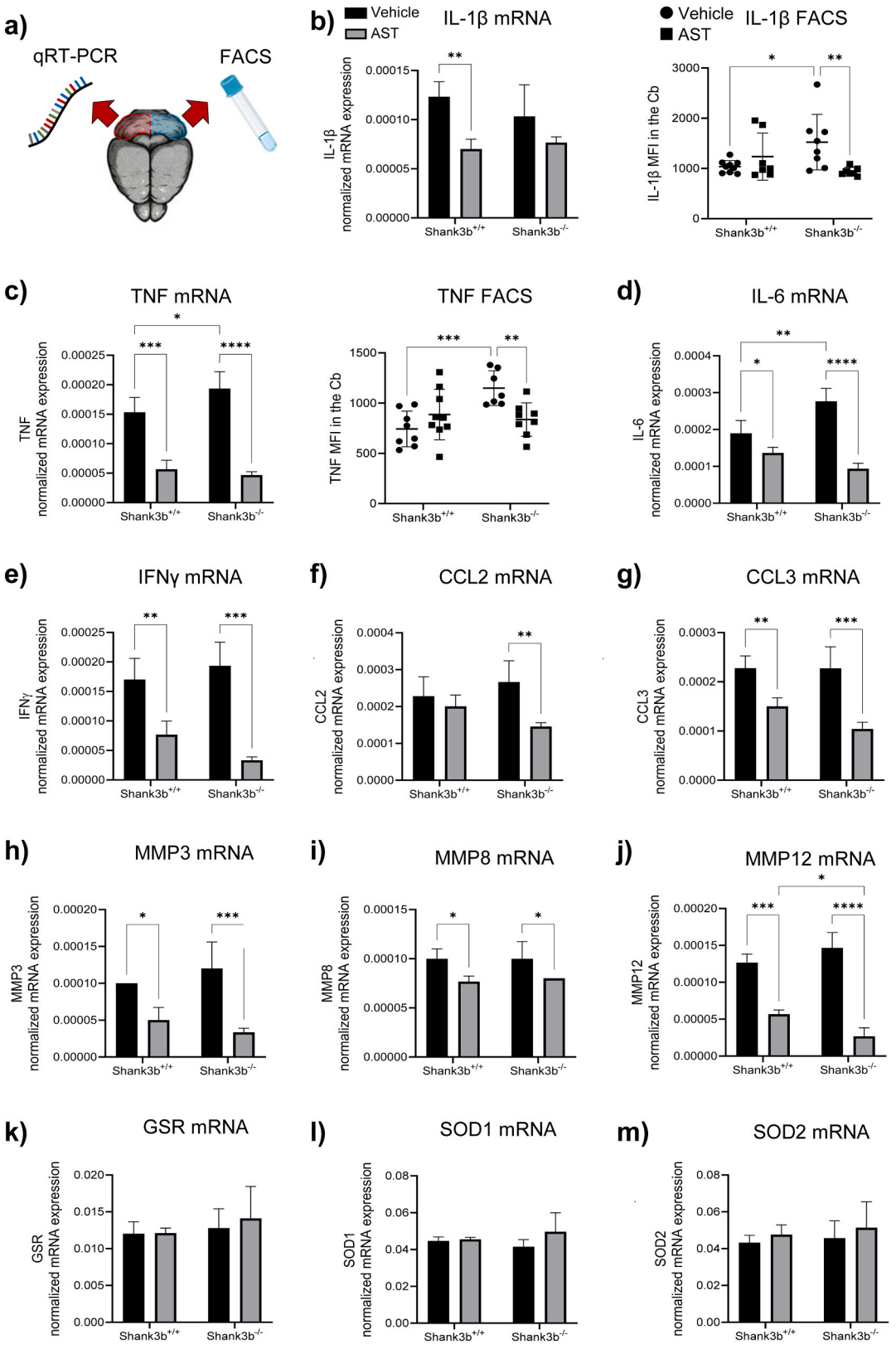

Fig. 2. Pro-inflammatory molecules in the cerebellum of *Shank3b*$^{+/+}$, and *Shank3b*$^{-/-}$ mice treated with AST (a) Chart showing a summary of the experimental design. Expression of (**b**) IL-1β and (**c**) TNF in the cerebellum of AST-treated *Shank3b*$^{+/+}$ and *Shank3b*$^{-/-}$ mice and vehicle-treated control animals measured at the mRNA level using qRT-PCR and at the protein level using flow cytometry (shown as mean fluorescence intensity, MFI). mRNA expression of (**d**) IL-6, (**e**) IFNγ, (**f**) CCL2, (**g**) CCL3, (**h**) MMP3, (**i**) MMP8, (**j**) MMP12, (**k**) GSR, (**l**) SOD1, and (**m**) SOD2 in the cerebellum of AST-treated and control animals. n = 8 in each group (for qRT-PCR), n = 8 (*Shank3b*$^{+/+}$, vehicle), n = 9 (*Shank3b*$^{+/+}$, AST), n = 7 (*Shank3b*$^{-/-}$, vehicle), n = 8 (*Shank3b*$^{-/-}$, AST). Two-way ANOVA, Tukey post-hoc test. *p < 0.05; **p < 0.01, ***p < 0.001, ****p < 0.0001. Data are expressed as Mean ± SD.

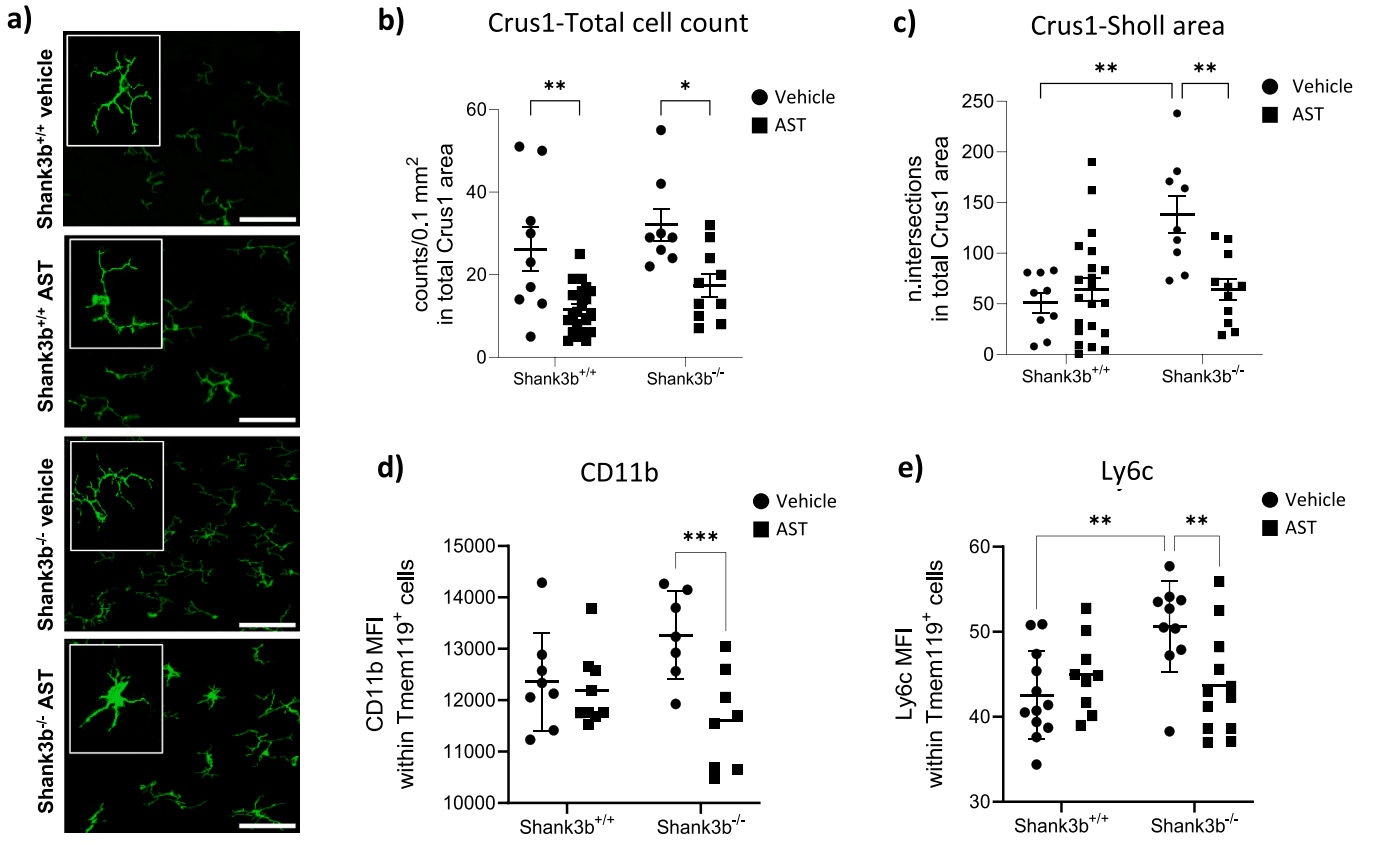

Fig. 3. Effects of AST on microglia in the cerebellum of *Shank3b*$^{+/+}$, and *Shank3b*$^{-/-}$ mice (a) Representative pictures showing microglia (iba-1^{+}) cells in the Crus1 area in the cerebellum of AST-treated *Shank3b*$^{+/+}$ and *Shank3b*$^{-/-}$ mice and vehicle-treated controls. Scalebar = 500 μm. (**b**) Cell number quantification (expressed in cells/0.1 mm^2) in the total Crus1 area. **(c)** Intersections of iba-1^{+} cells calculated with the Sholl analysis. For cell counting: n = 9 (*Shank3b*$^{+/+}$, vehicle), n = 22 (*Shank3b*$^{+/+}$, AST), n = 9 (*Shank3b*$^{-/-}$, vehicle), n = 12 (*Shank3b*$^{-/-}$, AST). For Sholl analysis: n = 9 (*Shank3b*$^{+/+}$, vehicle), n = 21 (*Shank3b*$^{+/+}$, AST), n = 9 (*Shank3b*$^{-/-}$, vehicle), n = 11 (*Shank3b*$^{-/-}$, AST). Mean fluorescence intensity (MFI) of (**d**) Cd11b, and (**e**) Ly6c in Tmem119^{+} cells. n = 7–12 (*Shank3b*$^{+/+}$, vehicle), n = 9 (*Shank3b*$^{+/+}$, AST), n = 10 (*Shank3b*$^{-/-}$, vehicle), n = 8–12 (*Shank3b*$^{-/-}$, AST). Two-way ANOVA, Tukey post-hoc test. $p < 0.05$; **$p < 0.01$, ***$p < 0.001$. Data are expressed as Mean ± SD.

(Fig. 4a). Nonetheless, IL-1β expression in BM T cells was reduced in *Shank3b*$^{-/-}$ mice administered with AST, while no differences were detected in CD14^{+} cells (data not shown). In parallel, TNF levels were markedly downregulated following AST treatment, both at the mRNA and protein levels within T cells, in *Shank3b*$^{+/+}$ and *Shank3b*$^{-/-}$ mice (Fig. 4b). Consistent results were also observed for TNF expression in BM CD14^{+} cells (Fig. S2a). Moreover, IL-6 and IFNγ mRNA levels were decreased in both genotypes after AST treatment, while protein expression was selectively reduced in T cells of *Shank3b*$^{-/-}$ mice for IL-6, and in T cells of both mutant and *Shank3b*$^{+/+}$ mice for IL-6 and IFNγ (Fig. 4c,d). Comparable trends were observed for chemokines and MMPs, except for MMP8, whose expression was increased in *Shank3b*$^{+/+}$ mice following AST administration but remained unchanged in *Shank3b*$^{-/-}$ animals (Fig. 4e–i). Furthermore IL-2 levels, which were elevated in T cells of vehicle-treated *Shank3b*$^{-/-}$ mice, were reduced in mutants upon AST treatment (Fig. S2b). In parallel, the levels of the antioxidant enzymes GSR, SOD1, and SOD2 were modulated by AST in both *Shank3b*$^{+/+}$ and *Shank3b*$^{-/-}$ mice (Fig. 4k–m). Specifically, while GSR and SOD2 were reduced in both genotypes, SOD1 decreased in *Shank3b*$^{+/+}$ mice but slightly increased in *Shank3b*$^{-/-}$ animals. Taken together, this data indicates that AST treatment can modulate and partially normalize the levels of pro-inflammatory molecules in the BM of both *Shank3b*$^{-/-}$ and *Shank3b*$^{+/+}$ mice.

2.4. Astaxanthin regulates the expression of molecules related to inflammation in the spleen and peripheral blood of Shank3b$^{-/-}$ *and Shank3b*$^{+/+}$ *mice*

We next investigated the effects of AST treatment on the expression of molecules related to inflammation in the spleen, an immunological organ that plays a key role in orchestrating systemic immune responses (Fig. 5). While AST had no significant effect in *Shank3b*$^{+/+}$ mice, increased IL-1β mRNA levels were observed in *Shank3b*$^{-/-}$ animals treated with AST (Fig. 5a). Similar results were found when the expression was measured at the protein level after stimulation within T cells. In parallel, TNF expression was substantially increased by the treatment in *Shank3b*$^{+/+}$ animals, whereas the levels of this cytokine were decreased in mutant mice, at least at the mRNA level (Fig. 5b). Similar trends were identified for IL-6 and IFNγ mRNAs, and therefore both cytokines were elevated in AST-treated *Shank3b*$^{+/+}$ mice compared to their oil-treated controls, while *Shank3b*$^{-/-}$ animals administered with AST showed reduced expression of these molecules when compared to controls (Fig. 5c,d). In stimulated T cells, both IL-6 and IFNγ were elevated in AST-treated *Shank3b*$^{-/-}$ animals in comparison with mutant controls, while IL-6 was additionally increased in the *Shank3b*$^{+/+}$ group administered with AST. Similar results were observed for the chemokines CCL2, CCL3, MMP3, and MMP12 and antioxidant enzymes GSR, SOD1 and SOD2 in the spleen of both genotypes following treatment (Fig. 5e–l). Notably, MMP8 showed divergent trends, being reduced in AST-treated *Shank3b*$^{-/-}$ mice and unchanged in *Shank3b*$^{+/+}$ animals. Additionally, IL-2 expression in T cells was increased in mutant mice

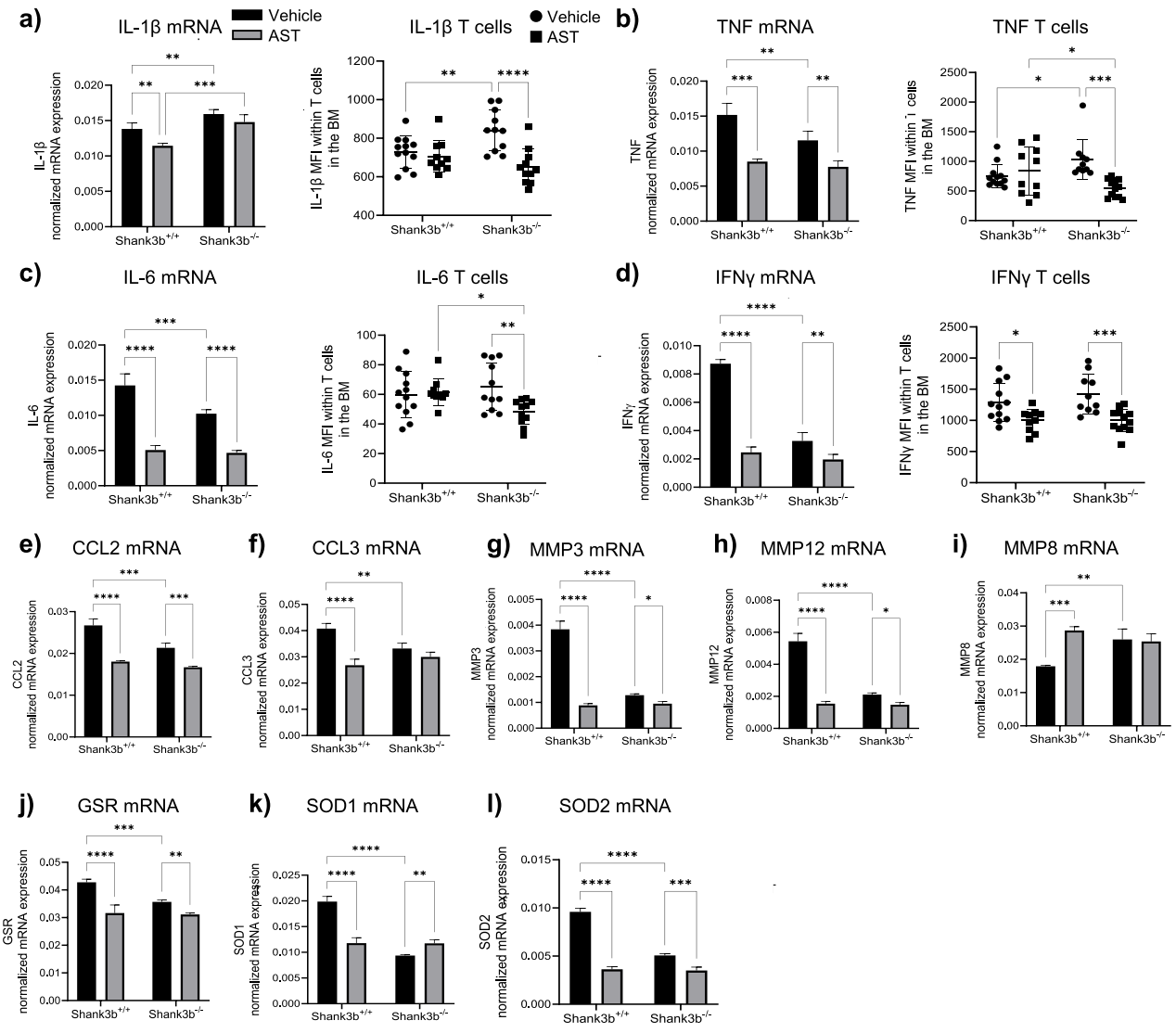

Fig. 4. Pro-inflammatory molecules in the bone marrow of *Shank3b*$^{+/+}$, and *Shank3b*$^{-/-}$ mice treated with AST Expression of (**a**) IL-1β, (**b**) TNF, (**c**) IL-6, and (**d**) IFNγ in the bone marrow (BM) of AST-treated *Shank3b*$^{+/+}$ and *Shank3b*$^{-/-}$ mice and vehicle-treated control animals measured at the mRNA level using qRT-PCR and at the protein level within T cells using flow cytometry (shown as mean fluorescence intensity, MFI). mRNA expression of (**e**) CCL2, (**f**) CCL3, (**g**) MMP3, (**h**) MMP12, and (**i**) MMP8, (**j**) GSR, (**k**) SOD1, and (**l**) SOD2 in the BM of AST-treated and control animals. n = 8 in each group (for qRT-PCR), n = 10–12 (*Shank3b*$^{+/+}$, vehicle), n = 10–12 (*Shank3b*$^{+/+}$, AST), n = 10–11 (*Shank3b*$^{-/-}$, vehicle), n = 10–12 (*Shank3b*$^{-/-}$, AST). Two-way ANOVA, Tukey post-hoc test. *p < 0.05; **p < 0.01, ***p < 0.001, ****p < 0.0001. Data are expressed as Mean ± SD.

administered with AST (Fig. S2c).

We finally assessed whether AST may additionally regulate the expression of pro-inflammatory molecules in PB mononuclear cells (PBMCs) of *Shank3b*$^{-/-}$ and *Shank3b*$^{+/+}$ mice (Fig. 6). Overall, the treatment did not change the frequencies of immune cell populations within PBMCs, except for a reduction in B cell frequencies observed in AST-treated *Shank3b*$^{+/+}$ animals (Figure S3). TNF expression in monocytes increased in mutant animals following AST treatment, while no differences were observed for *Shank3b*$^{+/+}$ mice (Fig. 6a). When TNF levels were analyzed within the whole T cell population and in CD4^{+} T cells, significant increases were detected in *Shank3b*$^{+/+}$ animals administered with AST in comparison with controls (Fig. 6b,c). Conversely, decreased TNF expression was found in CD4^{+} T cells of AST-treated mutant mice. No significant changes were induced by the drug within CD8^{+} T cells from either *Shank3b*$^{-/-}$ or *Shank3b*$^{+/+}$ mice (Fig. 6d). Similarly, IFNγ expression in T cells, as well as in CD4^{+} and CD8^{+} T cell subsets, was increased in *Shank3b*$^{+/+}$ animals treated with AST, when compared with controls (Fig. 6e-h). Again, the expression of this cytokine was reduced in AST-treated mutant animals, in CD4^{+} and CD8^{+} T cells (Fig. 6f,h). Additionally, IL-2 levels increased following AST administration in T cells from *Shank3b*$^{+/+}$ mice but decreased in the *Shank3b*$^{-/-}$ group. Taken together, AST treatment differentially modulates the expression of pro-inflammatory cytokines in PBMCs and spleen of *Shank3b*$^{-/-}$ or *Shank3b*$^{+/+}$ mice.

2.5. ROC analysis identifies cytokines with high discriminatory power in *Shank3b*$^{-/-}$ and *Shank3b*$^{+/+}$ mice

To identify which markers best discriminate between AST-treated and control mice within each genotype in the BM, spleen, and PB of *Shank3b*$^{+/+}$ and *Shank3b*$^{-/-}$ mice, we performed receiver operating characteristic (ROC) curve analysis using the expression levels of pro-inflammatory markers within different immune cell populations (Table 1). By calculating the area under the curve (AUC), optimal cutoff values, and corresponding sensitivity and specificity, we quantitatively assessed the diagnostic performance of each marker. In the BM of

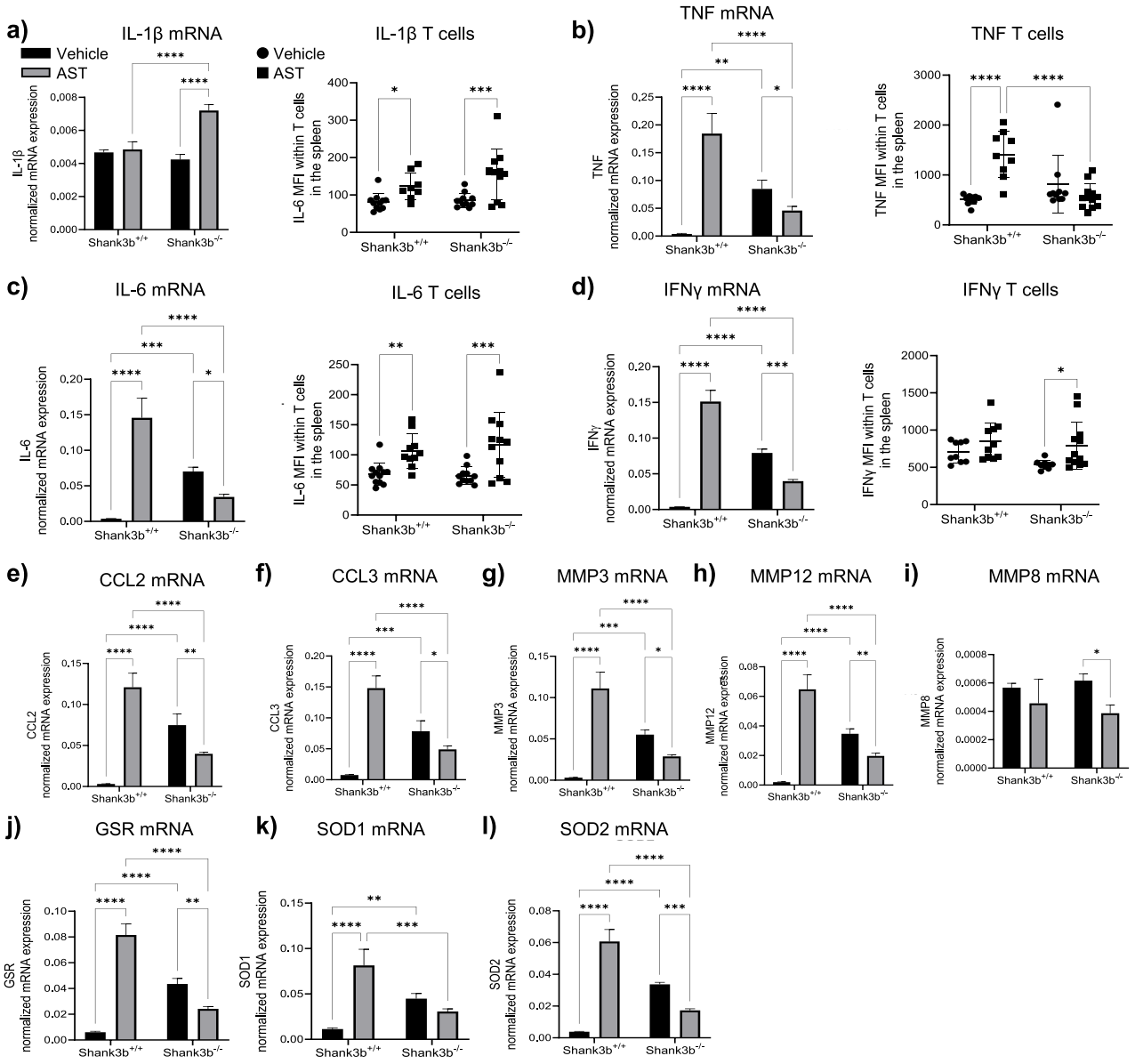

Fig. 5. Pro-inflammatory molecules in the spleen of *Shank3b*$^{+/+}$, and *Shank3b*$^{-/-}$ mice treated with AST Expression of (**a**) IL-1β, (**b**) TNF, (**c**) IL-6, and (**d**) IFNγ in the spleen of AST-treated *Shank3b*$^{+/+}$ and *Shank3b*$^{-/-}$ mice and vehicle-treated control animals measured at the mRNA level using qRT-PCR and at the protein level within T cells using flow cytometry (shown as mean fluorescence intensity, MFI). mRNA expression of (**e**) CCL2, (**f**) CCL3, (**g**) MMP3, (**h**) MMP12, (**i**) MMP8, (**j**) GSR, (**k**) SOD1, and (**l**) SOD2 in the spleen of AST-treated and control animals. n = 8 in each group (for qRT-PCR), n = 10–12 (*Shank3b*$^{+/+}$, vehicle), n = 10–12 (*Shank3b*$^{+/+}$, AST), n = 10–11 (*Shank3b*$^{-/-}$, vehicle), n = 10–12 (*Shank3b*$^{-/-}$, AST). Two-way ANOVA, Tukey post-hoc test. *$p < 0.05$; **$p < 0.01$, ***$p < 0.001$, ****$p < 0.0001$. Data are expressed as Mean ± SD.

Shank3b$^{-/-}$ animals, high discriminatory power was observed for TNF T cells, TNF CD8$^+$ T cells, IL-2 T cells, IL-1β T cells, and IL-1β CD4$^+$ T cells (AUCs ranging from 0.92 to 0.99), with TNF T cells and IL-1β CD4$^+$ T cells reaching near-perfect sensitivity and specificity (100/90 and 100/91, respectively). In contrast, *Shank3b*$^{+/+}$ mice displayed lower AUCs and no statistically significant results. In the spleen, TNF T cells, TNF CD4$^+$ T cells, and TNF CD8$^+$ T cells showed particularly strong diagnostic performance in *Shank3b*$^{-/-}$ mice (AUC between 0.94 and 0.97). Again, no significant AUCs were found for *Shank3b*$^{+/+}$ animals. IFNγ expression additionally showed significant discriminative values in *Shank3b*$^{-/-}$ mice with IFNγ T cells (AUC = 0.90), and IFNγ CD4$^+$ T cells (AUC = 0.84). No significant results were found in *Shank3b*$^{+/+}$ animals. In the PB, TNF CD14$^+$ cells (AUC = 0.97) and IFNγ CD4$^+$ T cells (AUC = 0.92) emerged as robust markers to distinguish AST-treated from control *Shank3b*$^{-/-}$ mice. Similarly, TNF CD4$^+$ T cells (AUC = 0.91), and IFNγ CD8$^+$ T cells (AUC = 0.95) showed high performance. No effective discriminators were found for *Shank3b*$^{+/+}$ animals. Taken together, the expression of pro-inflammatory markers in the BM, spleen, and PB may discriminate *Shank3b*$^{-/-}$ mice administered with AST from controls. Moreover, these results suggest that certain cytokines could serve as valuable biomarkers to monitor the efficacy of AST treatment.

2.6. Pro-inflammatory cytokines may be associated with parameters of behavioural tests

We next assessed whether the expression of pro-inflammatory cytokines in the BM, spleen, PB, and cerebellum correlated with parameters of behavioural tests (Table 2). IL-1β expression in BM CD4$^+$ T cells was negatively associated with the time spent on the rotarod. Although no significant differences were observed in the spleen, PB, and cerebellum,

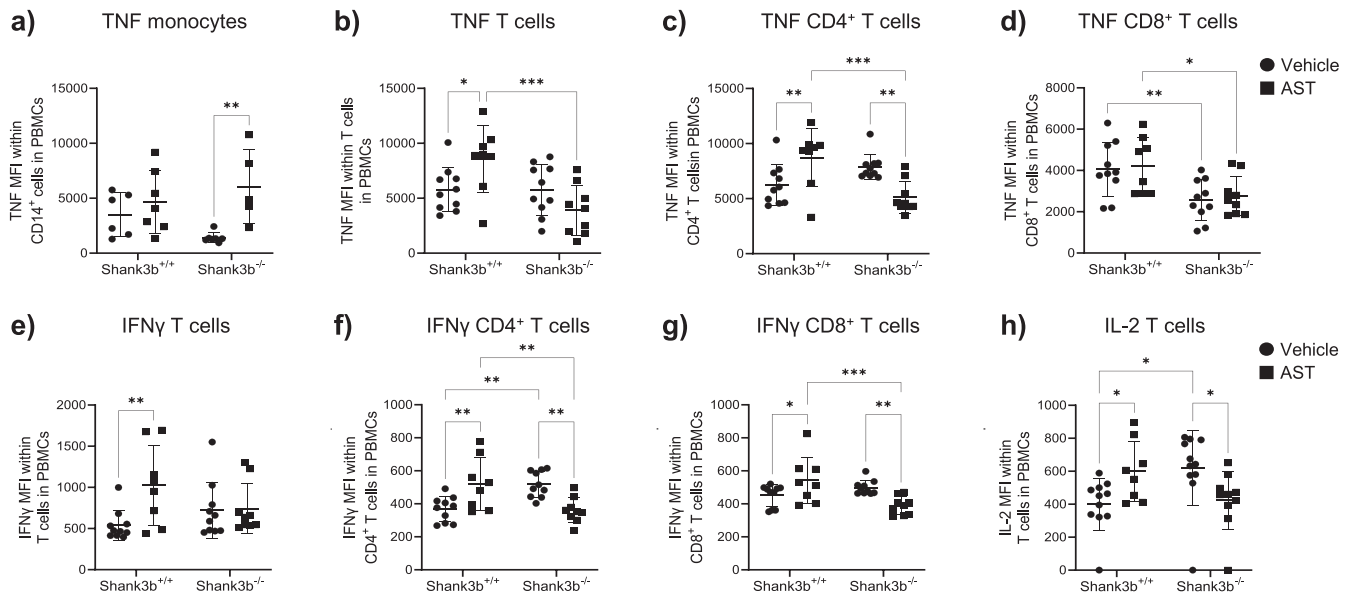

Fig. 6. Pro-inflammatory molecules in the peripheral blood of *Shank3b*$^{+/+}$, and *Shank3b*$^{-/-}$ mice treated with AST Expression of TNF within (**a**) monocytes (CD14$^+$ cells), (**b**) T cells, (**c**) CD4$^+$ T cells, and (**d**) CD8$^+$ T cells in peripheral blood mononuclear cells (PBMCs) of AST-treated *Shank3b*$^{+/+}$ and *Shank3b*$^{-/-}$ mice and vehicle-treated controls measured using flow cytometry. Expression of IFNγ within (**e**) T cells, (**f**) CD4$^+$ T cells, and (**g**) CD8$^+$ T cells, and (**h**) levels of IL-2 in T cells in the 4 groups. n = 6–12 (*Shank3b*$^{+/+}$, vehicle), n = 7–11 (*Shank3b*$^{+/+}$, AST), n = 6–11 (*Shank3b*$^{-/-}$, vehicle), n = 6–11 (*Shank3b*$^{-/-}$, AST). Two-way ANOVA, Tukey post-hoc test. *p < 0.05; **p < 0.01, ***p < 0.001. Data are expressed as Mean ± SD.

Table 1
Results of the ROC analysis in the BM, spleen and PB of *Shank3b*$^{+/+}$ and *Shank3b*$^{-/-}$ mice.

	Shank3b$^{+/+}$				*Shank3b*$^{-/-}$			
BM	AUC	p value	cutoff value	Sens/Spec (%)	AUC	p value	cutoff value	Sens/Specif (%)
TNF CD14$^+$ cells	**0.78**	**0.025**	**427**	**40/92**	**0.92**	**0.001**	**441**	**67/90**
TNF T cells	0.51	0.95	594	40/92	**0.99**	**< 0.0001**	**811**	**100/90**
IFNγ T cells	**0.76**	**0.04**	**980**	**40/92**	**0.89**	**0.002**	**1125**	**83/90**
TNF CD8$^+$ T cells	0.63	0.29	343	40/92	**0.92**	**0.001**	**354**	**75/90**
IL-2 T cells	0.70	0.12	235	40/92	**0.92**	**0.0008**	**257**	**67/90**
IL-1β T cells	0.60	0.41	703	70/75	**0.92**	**0.0009**	**706**	**82/91**
IL-1β CD4$^+$ T cells	0.52	0.84	944	60/58	**0.97**	**0.0002**	**1214**	**100/91**
IL-6 CD14$^+$ cells	0.54	0.74	58	90/50	**0.81**	**0.0138**	**47**	**45/90**
spleen								
TNF CD14$^+$ cells	**0.82**	**0.016**	**651**	**70/90**	**0.81**	**0.0147**	**709**	**83/80**
TNF T cells	**0.79**	**0.028**	**589**	**70/90**	**0.94**	**0.0006**	**809**	**83/89**
TNF CD4$^+$ T cells	0.75	0.059	633	60/90	**0.97**	**0.0003**	**867**	**92/89**
TNF CD8$^+$ T cells	0.63	0.33	539	70/70	**0.95**	**0.0005**	**865**	**83/89**
IFNγ T cells	0.69	0.17	861	40/89	**0.90**	**0.0022**	**569**	**83/89**
IFNγ CD4$^+$ T cells	0.54	0.76	672	20/90	**0.84**	**0.009**	**436**	**67/89**
IFNγ CD8$^+$ T cells	0.51	0.91	532	90/40	0.63	0.32	521	42/89
IL-2 T cells	0.68	0.17	197	40/90	0.65	0.24	251	42/89
PB								
TNF CD14$^+$ cells	0.64	0.39	5379	43/83	**0.97**	**0.0074**	**1844**	**100/86**
TNF T cells	0.77	0.05	8090	75/90	**0.73**	**0.08**	**2788**	**44/90**
TNF CD4$^+$ T cells	0.76	0.06	8470	75/90	**0.91**	**0.0025**	**6987**	**78/90**
TNF CD8$^+$ T cells	0.57	0.67	2532	100/33	0.75	0.17	2758	80/71
IFNγ T cells	0.84	0.016	699	75/90	0.56	0.68	1125	22/90
IFNγ CD4$^+$ T cells	0.79	0.04	458	63/90	**0.92**	**0.0022**	**421**	**78/90**
IFNγ CD8$^+$ T cells	0.73	0.11	505	63/90	**0.95**	**0.0009**	**463**	**89/90**

similar trends were described in the PB. Similarly, negative correlations were identified between the expression of pro-inflammatory cytokines in the BM—specifically IFN-γ in T cells, IL-1β in T cells, and IL-1β in CD4$^+$ T cells—and social behaviour as measured by the social index. Conversely, positive correlations were observed between grooming behaviour and IFN-γ expression in BM T cells, as well as TNF levels in T cell subsets in the spleen. Notably, a negative correlation between grooming and TNF levels in CD14$^+$ cells and T cells in the PB was also detected. Again, no significant associations were found in the cerebellum. Taken together, these findings suggest that the expression of pro-inflammatory cytokines in peripheral immune compartments may be related to behavioural parameters.

3. Discussion

Mice lacking the *Shank3b* gene robustly manifest autistic-like behaviours including social interaction deficits, repetitive behaviours, and motor impairments [1,17]. In this study, we showed that AST treatment

Table 2
Correlations between pro-inflammatory molecules and parameters of behavioural tests.

	Time on rotarod			Social index			Grooming		
	r_P	p	95 % confid.	r_P	p	95 % confid.	r_P	p	95 % confid.
BM									
TNF CD14$^+$ cells	-0.10	0.53	-0.39–0.22	-0.05	0.76	-0.35–0.26	0.20	0.19	-0.10–0.47
TNF T cells	-0.04	0.82	-0.34–0.28	-0.13	0.42	-0.42–0.19	0.04	0.82	-0.05–0.51
IFNγ T cells	0.14	0.38	-0.19–0.42	**-0.40**	**0.01**	-0.63 to −0.10	**0.50**	**0.001**	0.23–0.69
TNF CD8$^+$ T cells	-0.03	0.85	-0.33–0.28	0.04	0.81	-0.27–0.34	0.01	0.97	-0.29–0.30
IL-2 T cells	-0.05	0.77	-0.39–0.23	-0.15	0.34	-0.44–0.16	0.25	0.10	-0.05–0.51
IL-1β T cells	-0.15	0.34	-0.43–0.16	**-0.35**	**0.03**	-0.59 to −0.04	-0.11	0.47	-0.05–0.51
IL-1β CD4$^+$ T cells	**-0.33**	**0.03**	-0.57 to −0.03	**-0.47**	**0.002**	-0.68 to −0.18	-0.09	0.57	-0.38–0.22
IL-6 CD14$^+$ cells	0.22	0.15	-0.08 to −0.49	-0.29	0.07	-0.56 to −0.006	0.08	0.62	-0.23–0.36
spleen									
TNF CD14$^+$ cells	-0.13	0.39	-0.42–0.17	-0.16	0.31	-0.45–0.16	0.14	0.37	-0.17–0.42
TNF T cells	-0.01	0.93	-0.31–0.29	-0.15	0.34	-0.45–0.16	**0.34**	**0.02**	0.05–0.58
TNF CD4$^+$ T cells	-0.19	0.21	-0.46–0.11	-0.29	0.07	-0.55–0.03	**0.49**	**0.001**	0.23–0.69
TNF CD8$^+$ T cells	0.04	0.82	-0.27–0.33	-0.27	0.10	-0.53–0.05	**0.45**	**0.002**	0.17–0.66
IFNγ T cells	-0.03	0.85	-0.31–0.29	-0.14	0.39	-0.55–0.03	-0.17	0.29	-0.50–0.07
IFNγ CD4$^+$ T cells	0.04	0.80	-0.26–0.33	-0.12	0.48	-0.55–0.03	-0.21	0.18	-0.50–0.07
IFNγ CD8$^+$ T cells	0.06	0.69	-0.24–0.36	-0.11	0.51	-0.40–0.21	-0.17	0.29	-0.44–0.14
IL-2 T cells	-0.04	0.81	-0.35–0.25	0.21	0.20	-0.11–0.49	-0.25	0.10	-0.51–0.05
PB									
TNF CD14$^+$ cells	-0.05	0.79	-0.38–0.30	0.24	0.19	-0.12–0.54	**-0.45**	**0.01**	-0.68 to −0.14
TNF T cells	-0.25	0.16	-0.54–0.10	0.16	0.37	-0.19–0.48	**-0.35**	**0.04**	-0.61 to −0.02
TNF CD4$^+$ T cells	-0.27	0.12	-0.56–0.07	0.09	0.62	-0.26–0.42	-0.21	0.24	-0.50 to −0.14
TNF CD8$^+$ T cells	-0.06	0.74	-0.40–0.27	0.15	0.41	-0.26–0.42	-0.29	0.10	-0.57 to −0.05
IFNγ T cells	-0.29	0.09	-0.57–0.05	-0.04	0.82	-0.20–0.47	-0.23	0.18	-0.53–0.10
IFNγ CD4$^+$ T cells	-0.32	0.06	-0.59–0.02	0.06	0.72	-0.26–0.42	0.03	0.87	-0.31–0.35
IFNγ CD8$^+$ T cells	-0.15	0.39	-0.46–0.19	0.09	0.60	-0.26–0.42	-0.11	0.53	-0.43–0.23
Cb									
TNF CD14$^+$ cells	0.32	0.08	-0.04–0.60	-0.12	0.53	-0.47–0.25	-0.23	0.21	-0.54 to −0.14
IL-1β CD14 + cells	-0.05	0.79	-0.40–0.31	-0.29	0.13	-0.59–0.09	0.21	0.25	-0.54 to −0.14
IL-6 CD14$^+$ cells	-0.08	0.65	-0.42–0.28	-0.08	0.70	-0.43–0.09	0.10	0.58	-0.26 to −0.44
TNF T cells	0.28	0.13	-0.08–0.57	-0.13	0.51	-0.47–0.25	-0.29	0.11	-0.59–0.07
IFNγ T cells	-0.10	0.60	-0.43–0.27	-0.11	0.58	-0.45–0.27	-0.15	0.42	-0.48–0.21

in these mice successfully rescued these key phenotypes, as measured by increased sociability in the three-chamber test, improved latency to fall in the rotarod assay, and decreased self-grooming frequency. In addition, we provided evidence that AST, characterized by potent antioxidant and anti-inflammatory properties, was able to modulate neuroimmune pathways critically implicated in ASD pathophysiology.

These results closely mirror and extend our previous findings obtained with the antioxidant NAC, which also improved ASD-associated behaviours in *Shank3b*$^{-/-}$ and *Cntnap2*$^{-/-}$ mice [20,21]. Importantly, this work advances beyond simple therapeutic substitution by: i) uniquely extending behavioural domains (AST ameliorates motor coordination, unaffected by NAC); ii) supporting immune rebalancing (genotype-dependent suppression of harmful inflammation while preserving protective immunity, in the BM and spleen, absent with NAC); iii) proposing explorative biomarker analyses (ROC and correlation analyses, indirectly linking peripheral expression of pro-inflammatory molecules to behavioural parameters).

Furthermore, unlike synthetic NAC, AST is a naturally occurring carotenoid found in foods, offering added clinical value through dietary accessibility. In addition, the beneficial effects of NAC were limited by adverse pro-oxidant and pro-inflammatory effects in wild-type controls. Notably, AST did not induce detrimental pro-inflammatory side effects in *Shank3b*$^{+/+}$ mice, which may underscore a superior safety profile that is likely attributable to distinct biochemical properties.

While NAC is effective as a precursor for glutathione and acts by directly neutralizing free radicals and promoting thiol homeostasis, it may exhibit pro-oxidant or reductive stress effects in wild-type animals, particularly at higher doses, due to its SH-dependent reactivity and capacity to disrupt redox equilibrium in cells with intact endogenous antioxidant systems [27]. In contrast, AST is a potent lipid-soluble carotenoid with superior antioxidant and anti-inflammatory potential at the membrane level, where it suppresses lipid peroxidation and modulates neuroimmune pathways critically implicated in ASD pathophysiology [28]. At the doses tested, AST does not induce detectable pro-inflammatory side effects in *Shank3b*$^{+/+}$ mice [28].

Importantly, AST's biochemical activity extends beyond classic antioxidant action. Indeed, it has been shown to modulate mitochondrial function and attenuate the release of pro-inflammatory cytokines including IL-6 by interfering with the NF-κB and STAT3 signalling pathways [28]. The capacity of AST to directly bind IL-6 and break the inflammatory feedback loop makes this molecule very distinct from NAC, whose anti-inflammatory action is predominantly indirect and reliant on redox modulation. These key differences may enable AST to provide robust neuroprotection without triggering compensatory increases in oxidative stress or reductive imbalance [29]. Importantly, several independent reports have demonstrated that orally or dietarily administered AST crosses the blood–brain barrier, accumulates in rodent brain areas and exert neuroprotective effects [30–32].

Alongside the behavioural improvements, AST concurrently attenuated neuroinflammatory markers in the cerebellum and exerted broad immunomodulatory effects in peripheral immune compartments including BM, spleen, and PB, highlighting a systemic mechanism of action. With our results, we can speculate that AST's behavioural benefits may be mediated at least partly via modulation of the neuroimmune axis, a mechanistic convergence increasingly recognized in ASD research [33].

The cerebellum is emerging as a key brain area involved in ASD, with numerous studies detailing neuroanatomical, molecular, and functional disturbances including microglial activation and increased expression of pro-inflammatory cytokines [34–36]. AST administration broadly downregulated these canonical neuroinflammatory mediators at both the mRNA and protein levels in *Shank3b*$^{-/-}$ mice, while also eliciting

similar albeit subtler effects in *Shank3b*$^{+/+}$ animals. This finding further highlights the key role of oxidative stress and inflammation in ASD pathogenesis and severity and corroborates the therapeutic relevance of targeting redox–immune dysregulation.

Importantly, AST reversed the hyper-ramified, hypertrophic morphology characteristic of activated microglia in mutant mice, restoring a more surveillant, ramified state. This morphological remodelling was accompanied by a reduction in the expression of microglial activation markers CD11b and Ly6c, indicating a shift towards a less reactive phenotype. Activation markers CD11b and Ly6c are widely utilized to delineate inflammatory and activation states in microglia [37]. CD11b is expressed on microglia, peripheral monocytes, and infiltrating macrophages, and its upregulation reflects a shift towards a more reactive or phagocytic state during CNS inflammation [38]. Ly6c expression differentiates between resting/resident and infiltrating/inflammatory subsets. High Ly6c levels are present in brain-resident myeloid cells, while its downregulation denotes maturation or transition to an anti-inflammatory state [39]. Upon neuroinflammatory challenges, as seen in ASD models and CNS injury, microglia and monocyte-derived cells express elevated CD11b and Ly6c. Given the key role of microglia in regulating synaptic connectivity and modulating neuronal excitability [40], AST-mediated improvement of microglial morphology and activation state may likely relate to the behavioural improvements, therefore highlighting the modulation of microglial phenotype as a potential therapeutic target in ASD. Despite this, the quantification of microglia cells in the cerebellum revealed no differences between *Shank3b*$^{-/-}$ and *Shank3b*$^{+/+}$ mice, aligning with prior reports indicating that microglia density per se may not reflect changes in their activation status in ASD models [41].

In addition to the brain, immune dysregulation in ASD extends to peripheral organs and the blood, where aberrant cytokine profiles and altered immune cell phenotypes have been documented in our previous work [20–22]. Our study shows that AST exerted organ-specific immunomodulatory effects. Emerging evidence supports a functional connection between the brain and BM through systemic immune signalling and cellular trafficking, constituting a neuroimmune axis that may be dysregulated in ASD [33,42]. Thus, neuroinflammation observed in the brain with ASD is generally paralleled by peripheral immune abnormalities, including the BM. BM-derived immune cells can infiltrate the CNS under conditions of blood-brain barrier disruption, potentially contributing to ongoing neuroimmune dysfunction [43]. Conversely, pro-inflammatory signals originating in the brain can influence BM haematopoiesis, skewing immune cell production toward pro-inflammatory phenotypes, thus establishing a bidirectional interplay [44]. Although direct research on the brain-BM axis in ASD is limited, these neuroimmune interactions are increasingly recognized as crucial for understanding ASD pathophysiology [33].

Our results show that, in the BM, AST suppresses pro-inflammatory cytokines, potentially protecting hematopoietic stem cell niches from the deleterious effects of chronic inflammation. This condition may promote the establishment of an environment supporting the generation of “healthy” immune cells, which is often disrupted in chronic pro-inflammatory states. Thus, this putative brain–BM communication raises the possibility that AST may modulate inflammation in the BM, therefore preserving peripheral immune homeostasis but also indirectly modulating neuroinflammatory processes in the brain. This may contribute to the behavioural improvements observed in *Shank3b*$^{-/-}$ mice. Further studies dissecting this neuroimmune crosstalk in ASD could open opportunities for integrated peripheral and central immune interventions to counteract the severity of ASD.

In the spleen, AST effects were more complex and highly dependent on the genotype. Pro-inflammatory markers were reduced or rebalanced in *Shank3b*$^{-/-}$ mice, suggesting that the drug may partially counteract the pathological inflammation characteristic of this ASD model. In contrast, these markers were generally more expressed in *Shank3b*$^{+/+}$ animals after AST treatments. This may reflect an enhanced state of immune surveillance, and an increased capability to respond to potential threats. This complex modulation reflects the spleen's role as a frontline immune organ in balancing pathogen responsiveness with regulation of immune activation.

In the PB, AST modulated cytokine expression selectively within T cell subsets. In particular, while TNF and IFNγ expression were increased in *Shank3b*$^{+/+}$ animals, these cytokines were reduced in mutant mice, further suggesting that AST may rebalance immune responses based on underlying pathology rather than broadly suppressing immunity. Discrepancies between mRNA and protein expression observed in these compartments can be interpreted considering that mRNA levels were measured in unstimulated cells (reflecting basal transcription), whereas protein levels were assessed after 4 h of stimulation with PMA, ionomycin, and brefeldin A (BFA). Therefore, once activated, cells may exhibit distinct responses at the protein level compared to their basal mRNA expression.

The modulation of antioxidant enzymes in the BM and spleen by AST suggests that the compound may regulate the mRNA expression of antioxidant enzymes in a genotype-dependent manner, likely reflecting the distinct basal oxidative environments of *Shank3b*$^{+/+}$ and *Shank3b*$^{-/-}$ mice. The overall reduction of GSR and SOD2 in the BM in both genotypes may indicate that AST may lower oxidative burden, thereby reducing the need for constitutive antioxidant defence. This is consistent with the notion that AST directly scavenges reactive oxygen species and stabilizes mitochondrial membranes, diminishing the demand for endogenous antioxidant activity [45]. Interestingly, AST produced opposite effects on the expression of pro-inflammatory molecules and antioxidant enzymes in the spleen depending on genotype. This bidirectional modulation is compatible with a homeostatic, context-dependent action of AST rather than a unidirectional induction or suppression of antioxidant and inflammatory systems. In the spleen of *Shank3b*$^{+/+}$ mice AST may act as a mild adaptive stimulus (hermetic effect) that transiently elevates antioxidant defences (via Nrf2-dependent transcription and/or altered cytokine signalling) to bolster immune surveillance. By contrast, in the spleen of *Shank3b*$^{-/-}$ mice, which display chronic pro-inflammatory and pro-oxidant signalling, AST may lower oxidative burden, therefore leading to a reduced expression of antioxidant enzymes.

In line with this, the observed increase in the expression of pro-inflammatory molecules in *Shank3b*$^{+/+}$ mice administered with AST may reflect a beneficial adaptive immune priming rather than harmful inflammation. This aligns with the dual immunomodulatory profile of the drug, which promotes protective Type 1 T helper (Th1) immune surveillance in healthy states while suppressing pathological inflammation in disease contexts. In any case, based on the current data, immune activation should not be equated with immune safety. Furthermore, our interpretation remains speculative in the absence of immune challenge models, longitudinal follow-up, or toxicity assessments.

The spleen and brain may communicate through a bidirectional axis involving neural and immune signalling, especially via sympathetic and parasympathetic (particularly the vagus nerve) nervous system. While the sympathetic branch modulates cytokine production in the spleen to tune inflammation, signals from the vagus nerve reduce the release of proinflammatory cytokines [46]. Notably, the spleen can also feedback to the brain through cytokines and neuroimmune messengers, thereby regulating neuroinflammation and cognitive processes in health and disease [47]. In *Shank3b*$^{-/-}$ mice, dysregulated spleen function and peripheral immune surveillance may amplify neuroinflammatory processes, influencing neural development, synaptic organization, and core ASD-related behaviours. Thus, AST may normalize the dysregulated spleen-brain axis, restoring balanced neuroimmune communication and potentially ameliorating both peripheral and central pro-inflammatory abnormalities.

AST shows divergent effects in BM, spleen, and PB, which may partly reflect differences in tissue bioavailability and local exposure to the

compound. These organs also differ markedly in their immunological functions, from hematopoietic output and inflammatory priming in the BM to antigen-driven immune responses and cytokine integration in the spleen. Compartment-specific outcomes therefore likely arise from the combined influence of differential AST accessibility and the unique immune environments of each tissue.

An added value of this study is the use of the ROC analysis to identify markers that may discriminate between AST-treated and untreated mice across immune compartments, in *Shank3b*$^{-/-}$ and *Shank3b*$^{+/+}$ mice. TNF and IFNγ expression in BM and spleen T cells of *Shank3b*$^{-/-}$ animals showed high AUC values, indicating excellent sensitivity and specificity in distinguishing treatment response. Importantly, pro-inflammatory markers in PBMCs, such as TNF expression in CD14^{+} cells and IFNγ expression in T cell subsets, exhibited very high discriminatory power. Therefore, these parameters may represent highly promising, minimally invasive biomarkers for tracking immune dysfunction and evaluating therapeutic efficacy in ASD. The identification of such peripheral biomarkers is particularly relevant given the heterogeneous nature of ASD, and patient stratification based on immune and oxidative stress profiles optimizes the possibility of therapeutic success. It is important to underline that results from ROC analysis are exploratory and hypothesis-generating, thus they require further validation. Despite this, these data encourage the exploration of blood immune parameters in human ASD cohorts undergoing antioxidant treatments.

Our findings indicate that the expression of pro-inflammatory cytokines in peripheral immune compartments, particularly the BM, may be associated with behavioural parameters. These relationships, linking elevated BM pro-inflammatory cytokines to impaired performance in behavioural tests, provide correlational evidence for a functional brain-BM axis. Despite this, the existence and directionality of such an axis remain unconfirmed and will need to be rigorously tested in future studies. While the spleen also exhibited some associations, these were generally less pronounced. The lack of significant correlations in the cerebellum suggests that peripheral immune activity, especially within the BM and to a lesser extent the spleen, may have a more direct or influential relationship with behavioural outcomes. This supports the notion that immune signals originating from these peripheral sites could be connected with brain function and behaviour, potentially through systemic inflammatory pathways or immune-brain communication mechanisms (Fig. 7). Future studies should further explore these links to clarify how peripheral inflammation modulates neurobehavioural processes.

Although both male and female mice were included in the study, our sample sizes per group were insufficient to perform statistically robust sex-stratified analyses. In our previous work on the *Shank3b* model (including NAC treatment), we did not observe sex-related differences in the expression of pro-inflammatory molecules or behavioural parameters after the treatment, supporting the biological relevance of combining sexes in this context.

The potent antioxidant and anti-inflammatory properties of AST are well-documented in multiple models of neurological and systemic diseases, and its safety profile may be favourable, as it is widely consumed as a dietary supplement and it is found naturally in seafood and microalgae [28,29,48]. Our findings support the potential of AST as a therapeutic adjunct in ASD, particularly for individuals displaying immune dysregulation and oxidative stress. As current pharmacological options fail to adequately address the core behavioural disabilities and immune abnormalities of ASD, natural compounds like AST present an attractive alternative or complement to existing treatments, with reduced risk of adverse effects. Moreover, the capacity of AST to modulate both central and peripheral immune pathways may additionally be beneficial in mitigating ASD-associated comorbidities including gastrointestinal disorders, epilepsy, anxiety, and cognitive impairments.

While the behavioural tests assessed core ASD-like behaviours, they did not address associated symptoms such as anxiety or cognitive flexibility. Furthermore, although immune and morphological changes in microglia were clearly shown, functional assays measuring synaptic dynamics and electrophysiological responses would strengthen the link between the modulation of microglia and behavioural rescue. Future investigations should explore the effects of AST administration starting earlier in development, as early intervention is known to promote better outcomes in neurodevelopmental disorders. The differential immune responses observed between genotypes also highlight the importance of genetic background in shaping treatment outcomes, underscoring the need for personalized therapeutic strategies that can be guided by the profiling of immune biomarkers.

4. Limitations

Morphological normalization of microglia was observed following treatment, but no functional readouts (e.g., phagocytosis, synaptic pruning assays) were assessed. Although morphological changes represent a promising indicator of neuroinflammatory resolution in our mouse model, morphological normalization alone does not necessarily imply functional recovery.

Future work incorporating functional microglial assays will be needed to confirm therapeutic restoration.

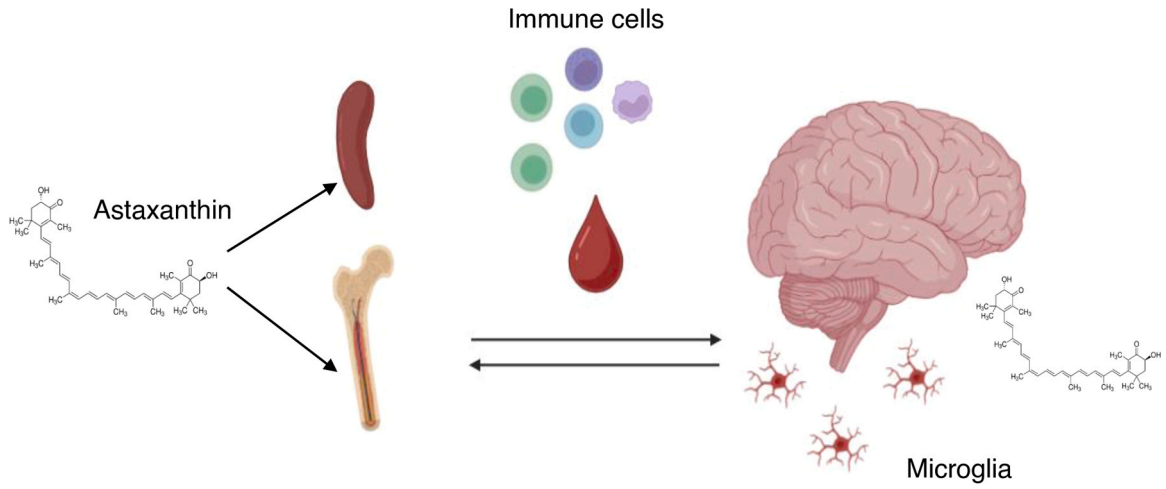

Fig. 7. Summary of the proposed mechanism of AST action on neuroimmune interactions. Schematic representation of the proposed mechanism of action of AST. AST may act on BM and splenic immune cells, which can subsequently migrate through the blood to the brain and modulate brain function and microglial activity. In parallel, AST can cross the blood–brain barrier and exert direct antioxidant and anti-inflammatory effects on neuronal cell types.

ROC-based biomarker analyses were conducted on relatively small sample sizes, rendering them exploratory in nature and susceptible to overfitting.These analyses will require validation in independent cohorts before predictive or translational applications. Future studies with larger datasets will confirm their robustness and generalizability.

The observed relationships linking elevated pro-inflammatory cytokines to impaired behavioural performance represent correlational evidence for a functional brain-BM axis, rather than direct causation. Ongoing analyses aim to generate more definitive mechanistic evidence.

Sex differences were not analyzed as a covariate or through treatment interaction tests due to insufficient sample sizes, which limits detection of potential sex-specific effects. Furthermore, exploratory sex-dependent analyses were not conducted. Future studies employing larger, balanced cohorts across sexes will be essential to evaluate these interactions comprehensively.

Although antioxidant enzymes were measured at the mRNA level, direct oxidative stress parameters (e.g., ROS levels, GSH/GSSG ratio, or SOD enzymatic activity) were not assessed. This absence of direct oxidative stress measurements represents a major limitation of this work; future studies with redox analyses must determine if transcriptional changes reflect functional shifts in oxidative status.

5. Material and methods

5.1. Animals

All experimental procedures were approved by the Animal Welfare Committee of the University of Trento and Italian Ministry of Health (protocol n.547/2021-PR), in accordance with the European Community Directive 2010/63/EU. Mice were housed following a 12 h light/dark cycle with food and water available *ad libitum*, taking care to minimize animal's pain and discomfort. Male and female *Shank3b*$^{-/-}$ and *Shank3b*$^{+/+}$ adult mice (3–5 months old; weight 25–35 g) obtained from heterozygous mating were used. Numbers of mice used for each experiment are reported in figure legends.

5.2. Experimental timeline and design

Animals were randomly assigned to treatment groups at the beginning of the experiment using a randomization table stratified by genotype, litter, and sex to ensure balance (equal males/females per group) and minimize bias. Blinding was implemented at two stages:

1) Post-treatment coding: After AST treatment completion, unique blinded codes were assigned to cages/animals by a technician uninvolved in experiments. 2) Analysis blinding: all behavioural and molecular analyses were performed using only codes. Group/genotype identities were revealed post-analysis by the same independent technician.

Shank3b$^{+/+}$ and *Shank3b*$^{-/-}$ mice were orally injected with 50 mg/kg natural AST (isolated from *Haematococcus pluvialis*, Sigma-Aldrich) dissolved in sunflower seed oil or vehicle (sunflower seed oil) 5 times/week for 4 consecutive weeks. Sex distribution was balanced across experimental groups. The optimal AST concentration to reduce brain inflammation was identified using available literature [49] and tested in preliminary experiments. Here, *Shank3b*$^{-/-}$ mice were treated with either 5 mg/kg or 50 mg/kg AST or remained untreated, and their performance on the rotarod test was assessed (Fig. 8). Three to four mice were included in each experimental group. The 50 mg/kg dose was selected as the only one that improved the performance of *Shank3b*$^{-/-}$ mice in the rotarod test.

Behavioural tests were performed during the last three days of AST treatment. Following the last behavioral assessment, brains, PB, BM, and spleen samples were collected and processed.

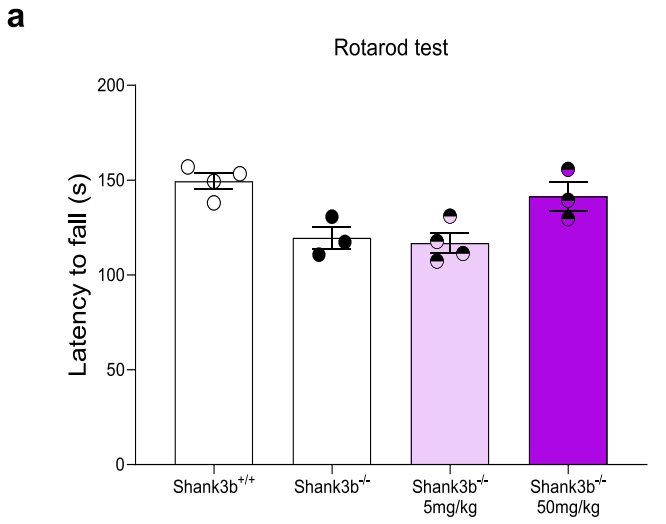

Fig. 8. Astaxanthin dose testing. a) Time on rotarod (latency to fall, s) in the rotarod test in vehicle-treated Shank3b$^{+/+}$ and Shank3b$^{-/-}$ mice and Shank3b$^{-/-}$ animals injected with 5 mg/kg or 50 mg/kg astaxanthin. n = 3–4 in each group.

5.3. Behavioural tests

Male and female mice were habituated and tested separately for all behavioural tests to avoid experimental noise. Observer bias was minimized by using automated measurements of the scores of behavioural assays. In the three-chamber social test, parameters were extracted with EthoVision XT, eliminating the need for manual scoring. Grooming behaviour and rotarod tests were scored from anonymized video recordings to ensure that the scorer was unaware of group identity. All behavioural tests were conducted consistently during the light phase between 8:00–12:00 AM under standard light-dark cycle conditions, with standardized timing maintained across all animals and treatment groups to minimize circadian variability.

5.3.1. Three-chamber social test

The three-chamber social test was used to quantify the social behaviours of mice as previously described [50]. The apparatus consisted of a rectangular plexiglass box [60x40x22(h) cm, each chamber 20x40x22(h) cm] with grayed walls and removable panels separating the box into three chambers. On the three days before the experimental phase, mice underwent a habituation session in which they were placed in the three-chamber apparatus and allowed to explore freely for 10 min. The experimental phase consisted of a 5-minute habituation session followed by a 10-minute exploration session. For the sociability test, an unfamiliar sex-matched mouse was secured within a wire cylindrical container (20 cm high, 10 cm diameter, 1 cm spaced bars) in one of the upper corners of an external chamber. A matching empty wire container was placed in the opposite external chamber. The tested mouse was permitted unrestricted interaction with both the social and empty objects for a total of 10 min. The time spent in the empty and social chambers and the sociability index [(time spent in the mouse chamber – time in the empty chamber) / total time in the external chambers] were used to assess the sociability of the tested mouse. The tests were recorded by an overhead camera placed over the apparatus. Mice were automatically video tracked using the EthoVisionXT software.

5.3.2. Rotarod test

Motor coordination dependent on cerebellar function was evaluated using the rotarod assay [51]. On the two days preceding the testing, mice were trained at a fixed rotational velocity of 4 revolutions per minute (rpm) to allow acclimatation. The experimental phase consisted

of three consecutive tests on the accelerating rod, in which the rotation gradually increased from 4 rpm to 64 rpm. Latency to fall was automatically recorded when the mouse landed on the metallic platform. For each mouse, the mean duration spent on the rod was calculated, serving as a quantitative measurement for balance and coordination performance on the accelerating apparatus.

5.3.3. Self-grooming assessment

To investigate repetitive and stereotypical behaviours of mice, self-grooming behaviours were evaluated using video recordings. Different forms of self-grooming behaviours, including flank/abdomen licking, face/snout wiping and rubbing, and stroking, were semi-automatically analyzed using the Boris software, allowing for systematic and objective measurement [52]. In this way, the frequency of self-grooming was calculated and analyzed.

5.3.4. Open field test

Open field test was performed to assess the motor activity of mice. Animals were placed in an empty open field arena (40 cm × 40 cm × 40 cm) and allowed to explore it freely for 10 min. Sessions were recorded by an overhead camera placed over the arena, and mice were automatically video tracked using the software EthoVisionXT (Noldus). Distance moved in the arena and mean velocity were analyzed.

5.4. Tissue harvesting

Cerebellar samples used for RT-PCR were dissected and frozen in dry ice. Cerebella used for the flow cytometry experiments were homogenized using a homogenizer immediately after dissections, and single-cell suspensions were prepared using Falcon 70μm cell strainers (Corning). Approximately two hundred μl of PB was harvested from each mouse and collected in a heparinized tube. PBMCs were isolated using a Ficoll-Hypaque density gradient (Sigma-Aldrich). BM cells were obtained after flushing femurs and tibias with PBS. Spleen samples were directly smashed through Falcon 70 μm cell strainers. After the isolation, cerebellum, BM, spleen cells and PBMCs were washed once with RPMI 1640 (Sigma-Aldrich) and resuspended in complete medium (RPMI 1640 supplemented with 10 % fetal calf serum, FCS, 100 U/mL penicillin and 100 μg/mL streptomycin; Sigma-Aldrich and Invitrogen respectively).

5.5. RNA isolation and quantitative RT-PCR (qRT-PCR)

Total RNAs were extracted from cerebellum, BM, and spleen samples of *Shank3b*$^{-/-}$, *Shank3b*$^{+/-}$, and *Shank3b*$^{+/+}$ mice using RNeasy Plus Mini Kit (Qiagen), and retro-transcribed to cDNA as reported in our previous work [12,43]. qRT-PCR was performed in a Bio-Rad C1000 Thermal Cycler, using the PowerUp™ SYBR™ Green Master Mix (Applied Biosystems). Primers (Eurofins Genomics) were designed on different exons to avoid amplification of genomic DNA. The sequences of primers used for the study are shown in Table 3. CFX3 Manager 3.0 (Bio-Rad) software was used for expression analysis. Mean cycle threshold (Ct) values from triplicate experiments were calculated for each gene of interest and the housekeeping gene β actin, and afterwards corrected for PCR efficiency and inter-run calibration. The expression of each mRNA of interest (normalized against β actin) was compared from triplicate experiments performed on RNA pools from 8 to 10 samples for each group.

5.6. Flow cytometry

Flow cytometry was used to quantify cytokine levels and assess the frequency of immune cell populations in the cerebellum, PB, BM, and spleen. Surface staining was performed by adding a panel of directly conjugated antibodies to freshly prepared cells. Dead cells were excluded from the analysis using fixable viability dye (FVD) (BD Biosciences). For the assessment of intracellular cytokines, cells were incubated with 30 ng/mL phorbol 12-myristate 13-acetate (PMA) and 500 ng/mL ionomycin in the presence of 10 mg/mL brefeldin A (BFA) (all molecules from Sigma-Aldrich) for 4 h at 37 °C, as previously done in our work [20–22]. After surface staining, cells underwent permeabilization using the Cytofix/Cytoperm kit (BD Biosciences), followed by incubation with antibodies targeting intracellular cytokines. Labeled cells were measured using a BD Fortessa flow cytometer (BD Biosciences), and the resulting data were processed using Flowjo software. The antibodies used in the experiments are shown in Table 4.

5.7. Immunofluorescence staining of cerebellar sections

Brains were excised, post-fixed overnight in 4 % paraformaldehyde (PFA) at 4°C, washed, and then transferred to a cryoprotectant solution (80 % PBS, 20 % glycerol with 0.1 % sodium azide), and stored at 4°C. Cryoprotected brains were embedded in 4 % agarose gel and sectioned sagitally on a vibratome (Leica, VT1200) at 40μm thickness. Sequential slices were collected in separate wells containing cryoprotectant

Table 4
Antibodies used for the flow cytometry experiments.

Antigen	Fluorocrome	Company	Clone
CD45	PE	Miltenyi	REA747
CD3	APC-Vio770	Miltenyi	REA641
CD4	VioGreen	Miltenyi	REA1211
CD8	PerCp	Biolegend	53–6.7
CD8	PE-Vio770	Miltenyi	REA601
CD19	PerCp	Miltenyi	REA749
B220	Vioblue v	Miltenyi	REA755
CD14	Pecy7	Biolegend	Sa14–2
IFNγ	FITC	Miltenyi	REA638
TNF	PE	Biolegend	MP6-XT22
IL-2	APC	Biolegend	JES6–5H4
IL-6	APC	Biolegend	MP5–20F3
IL-1β	PE	Miltenyi	REA577
Tmem119	Pecy7	ThermoF.	V3RT1GOsz
CD11b	APC-Vio770	Miltenyi	REA592
Ly6C	PerCp	Miltenyi	REA796

Table 3
Sequences of the primers used for this study.

Target gene	Forward primer (5'-3')	Reverse primer (5'-3')
TNF	CAAAATTCGAGTGACAAGCC	TGTCTTTGAGATCCATGCCG
IFNγ	CCCTATGGAGATGACGGAGA	CTGTCTGCTGGTGGAGTTCA
IL-6	GCCTTCTTGGGACTGATGCT	GACAGGTCTGTTGGGAGTGG
IL-1β	ACGGACCCCAAAAGATGAAG	TTCTCCACAGCCACAATGAG
CCL2	CCAGCTTCGACCTAGCAGACA	CAGCGTGGCTGATGGTTGTA
CCL3	TGAAACCAGCAGCCTTTGCT	AGGCATTCAGTTCCAGGTCAGTG
MMP3	CAGACTTGTCCCGTTTCCAT	GGTGCTGACTGCATCAAAGA
MMP8	AATCCTTGCCCATGCCTTTCAACC	CCAAATTCATGAGCAGCCACGAGA
MMP12	GGAGCTCACGGAGACTTCAACT	CCTTGAATACCAGGTCCAGGATA
β actin	GGCTGTATTCCCCTCCATCG	CCAGTTGGTAACAATGCCATGT

solution.

Free-floating sections were first rinsed in PBS and washed three times in PBS containing 0.2 % Triton X-100 for 10 min each. Tissue slices were then incubated for 3 h at room temperature in blocking buffer (10 % FCS, 1 % BSA, 0.3 % Triton X-100 in PBS). After one PBS wash (10 min), slices were incubated overnight (16–18 h) at room temperature in primary antibody dilution buffer (3 % FCS, 1 % BSA, 0.1 % Triton X-100 in PBS) containing rabbit anti-Iba1 (1:750, Synaptic Systems). On the following day, sections were washed three times in PBS (10 min each) and incubated in the dark for 2 h at 4°C with Alexa Fluor 488-conjugated anti-rabbit secondary antibody (1:300, Life Technologies) diluted in secondary antibody buffer (5 % FCS, 1 % BSA in PBS). After three additional PB washes, sections were mounted on gelatin-coated Superfrost slides, air-dried, and cover-slipped with FluorSave mounting medium (Southern Biotech). Slides were stored at 4°C until they were imaged.

5.8. Image acquisition and microglia quantification

A Nikon Eclipse Ti2 spinning disc fluorescent microscope (Advanced Imaging Facility, Department of Cellular, Computational and Integrative Biology, CIBIO, University of Trento), equipped with a 40X/0.95 Plan Apochromatic Lambda D objective, was used to image the entire area of Crus1 and Crus2 in the cerebellum along the full x-, y-, and z-axes. Images were acquired with the following settings: Andor Zyla 4.2 PLUS sCMOS camera, 100 ms exposure time, 12-bit depth, gain 4, and a region of interest of 1702 × 1702 pixels. Excitation was achieved using the Celesta 477 nm laser line (for GFP) at 15 % power. The spinning disc acquisition mode employed a 70 μm pinhole size, with a z-step of 0.5 μm. Acquisition parameters were set during the first acquisition of the control experimental sample (*Shank3b*$^{+/+}$ oil) and kept constant for all subsequent images. The scale for fluorescence images taken at 20x magnification is derived from an image with the following metadata: a width and height of 283.07 μm (1702 pixels), a resolution of 6.01 pixels/μm, and a pixel size of 0.166 × 0.166 μm^2. All images were captured using the 40x/0.95 Plan Apochromatic Lambda D objective. Fluorophore excitation and emission settings were 493 nm / 537 nm for Alexa-488 and 600 nm / 670 nm for Alexa-594. Between one and four tissue sections per animal were imaged, and quantitative data were averaged. Between one and four sections per animal were acquired. For data analysis, values from all sections were averaged across these sections to represent each animal. All acquisitions were anonymized to avoid bias during both acquisition and analysis.

5.9. Analysis of microscope images

Images captured by confocal microscopy were processed and analyzed using Fiji-ImageJ software. Each image was first standardized by selecting an 80-stack z-interval, equivalent to a 40 μm tissue thickness. To enhance analysis consistency across experimental groups, each image has been pre-processed by performing background subtraction, sharpening using an unsharp mask, and noise removal using the Despeckle function in Fiji. Quantification of microglia cell numbers and Sholl analysis within Crus 1 and Crus 2 areas were performed on iba-1$^+$ cells.

5.9.1. Quantification of microglia cells

For microglial quantification, the entire Crus 1 and Crus 2 regions were scanned in three dimensions (x, y, z), with molecular and granular layers delineated via the ROI manager. Iba-1-positive cell bodies were manually counted using the cell-counter plugin, and densities were calculated as the number of somata per 0.1 mm^2 in individual layers and combined areas.

5.9.2. Sholl analysis of microglia cells

Sholl analysis was performed to evaluate microglial morphology. Iba-1$^+$ cells were selected using a grid of 13 size-matched squares. For each image, a total of 2 size-matched squares, one in the molecular and one in the granular layer, were alternatively displayed to ensure a random sampling of iba-1$^+$ cells within the areas of interest. Selected cells were extracted, then segmented and tracked using the ImageJ tool "microglia plugin". Thresholds were adjusted with erosion and dilation tools to refine segmentation before Sholl analysis, which quantified total branch intersections across concentric shells from each cell's soma, providing detailed morphological characterization. Sholl analysis was performed using the "Sholl Analysis plugin".

5.10. Statistics

Statistical analyses were performed using GraphPad Prism 8.0 software, using two-way ANOVA followed by a Tukey post-hoc test. Data were tested for normality and found to be normally distributed, thus justifying the use of parametric tests. Receiver Operating Characteristic (ROC) curve analyses were carried out to evaluate the diagnostic performance of immune cell markers in treated and control *Shank3b*$^{+/+}$ and *Shank3b*$^{-/-}$ mice. The area under the curve (AUC), optimal cutoff values, sensitivity, and specificity were derived from the ROC curves. To control false positives from multiple comparisons, FDR correction was performed. To evaluate the association between expression of pro-inflammatory molecules and parameters of behavioral tests, Pearson correlation analysis was performed. Statistical significance was set at $p < 0.05$. Exact p values and 95 % confidence intervals for Figs. 1–6 are reported in the Supplementary table 1.

Funding

This work was supported by the Autism Research Institute (ARI) 2023 Research Award to YB.

CRediT authorship contribution statement

Anjana Madhavan: Writing – review & editing, Visualization, Investigation, Data curation. **Martina Schiano-Visconte:** Investigation, Data curation. **Lauren Dutton:** Investigation. **Mattia Cantalupo:** Investigation. **Luigi Balasco:** Methodology, Investigation, Data curation. **Alessia Mavillonio:** Investigation. **Gabriele Chelini:** Writing – review & editing, Supervision, Methodology, Investigation. **Yuri Bozzi:** Writing – review & editing, Supervision, Resources, Funding acquisition. **Luca Pangrazzi:** Writing – original draft, Visualization, Validation, Supervision, Resources, Project administration, Methodology, Investigation, Formal analysis, Data curation, Conceptualization.

Declaration of Competing Interest

The authors declare that they have no known competing financial interests or personal relationships that could have appeared to influence the work reported in this paper.

Acknowledgements

The authors thank the technical and administrative staff of CIMeC, University of Trento, for excellent support. In addition, we thank the Biooptical Centre Facility of the Institute for Biomedical Aging Research (University of Innsbruck) coordinated by Brigitte Jenewein for the support in the flow cytometry experiments.

Appendix A. Supporting information

Supplementary data associated with this article can be found in the online version at doi:10.1016/j.biopha.2026.119051.

Data Availability

Some data have been deposited, the doi (https://doi.org/10.12751/g-node.q4qihq) has been included.

References

[1] American Psychiatric Association. Diagnostic and statistical manual of mental disorders, 5th ed., American psychiatric publishing: Washington, DC, USA, 2013.

[2] J. Zeidan, E. Fombonne, J. Scorah, A. Ibrahim, M.S. Durkin, S. Saxena, A. Yusuf, A. Shih, M. Elsabbagh, Global prevalence of autism: A systematic review update, Autism Res 15 (5) (2022) 778–790, https://doi.org/10.1002/aur.2696.

[3] J. Zeidan, E. Fombonne, J. Scorah, A. Ibrahim, M.S. Durkin, S. Saxena, A. Yusuf, A. Shih, M. Elsabbagh, Global prevalence of autism: A systematic review update, Autism Res 15 (5) (2022 May) 778–790, https://doi.org/10.1002/aur.2696.

[4] M.J. Maenner, Z. Warren, A.R. Williams, et al., Prevalence and Characteristics of Autism Spectrum Disorder Among Children Aged 8 Years — Autism and Developmental Disabilities Monitoring Network, 11 Sites, United States, 2020, MMWR Surveill. Summ. 72 (SS-2) (2023) 1–14, https://doi.org/10.15585/mmwr.ss7202a1.

[5] M.V.F. Holanda, E.D.S. Paiva, L.N. de Souza, K.M. Paiva, R.F. Oliveira, É.A. F. Tavares, P.L.A.G. Morais, A.M. de Andrade, M.I. Knackfuss, E.G.C. do Nascimento, J.R.L.P. Cavalcanti, Neurobiological basis of autism spectrum disorder: mini review, Front Psychol. 16 (2025 May 30) 1558081, https://doi.org/10.3389/fpsyg.2025.1558081.

[6] L. Pangrazzi, L. Balasco, Y. Bozzi, Oxidative stress and immune system dysfunction in autism spectrum disorders, Int J. Mol. Sci. 21 (9) (2020 May 6) 3293, https://doi.org/10.3390/ijms21093293.

[7] Y. Chen, X. Du, X. Zhang, F. Li, S. Yuan, W. Wang, Z. Zhu, M. Wang, C. Gu, Research trends of inflammation in autism spectrum disorders: a bibliometric analysis, Front Immunol. 16 (2025 Feb 14) 1534660, https://doi.org/10.3389/fimmu.2025.1534660.

[8] P. Ashwood, P. Krakowiak, I. Hertz-Picciotto, R. Hansen, I. Pessah, J. Van de Water, Elevated plasma cytokines in autism spectrum disorders provide evidence of immune dysfunction and are associated with impaired behavioural outcome, Brain Behav. Immun. 25 (1) (2011 Jan) 40–45, https://doi.org/10.1016/j.bbi.2010.08.003.

[9] M.C. Inga Jácome, L.M. Morales Chacòn, H. Vera Cuesta, C. Maragoto Rizo, M. Whilby Santiesteban, L. Ramos Hernandez, E. Noris García, M.E. González Fraguela, C.I. Fernandez Verdecia, Y. Vegas Hurtado, D. Siniscalco, C.A. Gonçalves, M.L. Robinson-Agramonte, Peripheral inflammatory markers contributing to comorbidities in autism, Behav. Sci. (Basel) 6 (4) (2016) 29, https://doi.org/10.3390/bs6040029.

[10] X. Liao, M. Chen, Y. Li, The glial perspective of autism spectrum disorder convergent evidence from postmortem brain and PET studies, Front Neuroendocr. 70 (2023 Jul) 101064, https://doi.org/10.1016/j.yfrne.2023.101064.

[11] L. Pangrazzi, L. Balasco, Y. Bozzi, Natural antioxidants: a novel therapeutic approach to autism spectrum disorders? Antioxid. (Basel) 9 (12) (2020 Nov 26) 1186, https://doi.org/10.3390/antiox9121186.

[12] L. Chen, X.J. Shi, H. Liu, X. Mao, L.N. Gui, H. Wang, Y. Cheng, Oxidative stress marker aberrations in children with autism spectrum disorder: a systematic review and meta-analysis of 87 studies (N = 9109), Transl. Psychiatry 11 (1) (2021) 15, https://doi.org/10.1038/s41398-020-01135-3.

[13] S. Rose, S. Melnyk, O. Pavliv, S. Bai, T.G. Nick, R.E. Frye, S.J. James, Evidence of oxidative damage and inflammation associated with low glutathione redox status in the autism brain, Transl. Psychiatry 2 (7) (2012) e134, https://doi.org/10.1038/tp.2012.61.

[14] X. Liu, J. Lin, H. Zhang, N.U. Khan, J. Zhang, X. Tang, X. Cao, L. Shen, Oxidative stress in autism spectrum disorder-current progress of mechanisms and biomarkers, Front Psychiatry 13 (2022) 813304, https://doi.org/10.3389/fpsyt.2022.813304.

[15] H.K. Hughes, R.J. Moreno, P. Ashwood, Innate immune dysfunction and neuroinflammation in autism spectrum disorder (ASD), Focus (Am. Psychiatr. Publ.) 22 (2) (2024 Apr) 229–241, https://doi.org/10.1176/appi.focus.24022004.

[16] R. Renaldi, A.M. Persico, T. Wiguna, A.J. Tanra, Breaking the cycle of oxidative stress for better behavioural health in autism spectrum disorder: a scoping review, Asian J. Psychiatr. 110 (2025 Aug) 104575, https://doi.org/10.1016/j.ajp.2025.104575.

[17] J. Peça, C. Feliciano, J.T. Ting, W. Wang, M.F. Wells, T.N. Venkatraman, C. D. Lascola, Z. Fu, G. Feng, Shank3 mutant mice display autistic-like behaviours and striatal dysfunction, Nature 472 (7344) (2011 Apr 28) 437–442, https://doi.org/10.1038/nature09965.

[18] L. Balasco, M. Pagani, L. Pangrazzi, G. Chelini, A.G. Ciancone Chama, E. Shlosman, L. Mattioni, A. Galbusera, G. Iurilli, G. Provenzano, A. Gozzi, Y. Bozzi, Abnormal Whisker-Dependent Behaviours and Altered Cortico-Hippocampal Connectivity in Shank3b-/- Mice, Cereb. Cortex 32 (14) (2022 Jul 12) 3042–3056, https://doi.org/10.1093/cercor/bhab399.

[19] K. Phelan, H.E. McDermid, The 22q13.3 deletion syndrome (Phelan-McDermid Syndrome), Mol. Syndr. 2 (2012) 186–201, https://doi.org/10.1159/000334260.

[20] L. Pangrazzi, E. Cerilli, L. Balasco, C. Khurshid, C. Tobia, G.M. Dall'O', et al., The interplay between oxidative stress and inflammation supports autistic-related behaviours in Cntnap2 knockout mice, Brain Behav. Immun. 127 (2025 Jul) 57–71, https://doi.org/10.1016/j.bbi.2025.02.030.

[21] L. Pangrazzi, E. Cerilli, L. Balasco, G.M. Dall'O', G. Chelini, A. Pastore, B. Weinberger, Y. Bozzi, N-acetylcysteine counteracts immune dysfunction and autism-related behaviours in the shank3b mouse model of autism spectrum disorder, Antioxid. (Basel) 13 (11) (2024 Nov 14) 1390, https://doi.org/10.3390/antiox13111390.

[22] E. Cerilli, G.M. Dall'O, G. Chelini, B. Catena, B. Weinberger, Y. Bozzi, L. Pangrazzi, Immune system dysfunction and inflammation in aging Shank3b mutant mice, a model of autism spectrum disorder, Front Immunol. 15 (2024 Sep 6) 1447385, https://doi.org/10.3389/fimmu.2024.1447385.

[23] P. Si, C. Zhu, Biological and neurological activities of astaxanthin (Review), Mol. Med Rep. 26 (4) (2022 Oct) 300, https://doi.org/10.3892/mmr.2022.12816.

[24] J.S. Park, J.H. Chyun, Y.K. Kim, L.L. Line, B.P. Chew, Astaxanthin decreased oxidative stress and inflammation and enhanced immune response in humans, Nutr. Metab. (Lond.) 7 (2010 Mar 5) 18, https://doi.org/10.1186/1743-7075-7-18.

[25] M.W. Abdallah, T.M. Michel, Matrix metalloproteinases in autism spectrum disorders, J. Mol. Psychiatry 1 (1) (2013 Sep 17) 16, https://doi.org/10.1186/2049-9256-1-16.

[26] M.S. Dukhinova, J. Guo, E. Shen, W. Liu, W. Huang, Y. Shen, L. Wang, Cerebellar microglia: On the edge between neuroinflammation and neuroregulation, Neural Regen. Res 21 (1) (2026 Jan 1) 156–172, https://doi.org/10.4103/NRR.NRR-D-24-00550.

[27] B. Pedre, U. Barayeu, D. Ezeriņa, T.P. Dick, The mechanism of action of N-acetylcysteine (NAC): The emerging role of H2S and sulfane sulfur species, Pharm. Ther. 228 (2021 Dec) 107916, https://doi.org/10.1016/j.pharmthera.2021.107916.

[28] M. Zuluaga, A. Barzegari, D. Letourneur, V. Gueguen, G. Pavon-Djavid, Oxidative Stress Regulation on Endothelial Cells by Hydrophilic Astaxanthin Complex: Chemical, Biological, and Molecular Antioxidant Activity Evaluation, Oxid. Med Cell Longev. 2017 (2017) 8073798, https://doi.org/10.1155/2017/8073798.

[29] P. Lobos, B. Bruna, A. Cordova, P. Barattini, J.L. Galáz, T. Adasme, C. Hidalgo, P. Muñoz, A. Paula-Lima, Astaxanthin Protects Primary Hippocampal Neurons against Noxious Effects of Aβ-Oligomers, Neural Plast. 2016 (2016) 3456783, https://doi.org/10.1155/2016/3456783.

[30] Y. Manabe, T. Komatsu, S. Seki, T. Sugawara, Dietary astaxanthin can accumulate in the brain of rats, Biosci. Biotechnol. Biochem 82 (8) (2018 Aug) 1433–1436, https://doi.org/10.1080/09168451.2018.1459467.

[31] B. Grimmig, S.H. Kim, K. Nash, P.C. Bickford, R. Douglas Shytle, Neuroprotective mechanisms of astaxanthin: a potential therapeutic role in preserving cognitive function in age and neurodegeneration, Geroscience 39 (1) (2017 Feb) 19–32, https://doi.org/10.1007/s11357-017-9958-x.

[32] A.S. Mohd Shafie, S.N. Kamarudin, M.M.R. Meor Mohd Affandi, R. Siran, Exploring astaxanthin: a comprehensive review on its pharmacokinetics properties and neuroprotective potential, Nutr. Neurosci. 28 (10) (2025 Oct) 1197–1224.

[33] J.M. Vacharasin, J.A. Ward, M.M. McCord, K. Cox, J. Imitola, S.B. Lizarraga, Neuroimmune mechanisms in autism etiology - untangling a complex problem using human cellular models, Oxf. Open Neurosci. 3 (2024 Feb 22) kvae003.

[34] C.J. Stoodley, A.M. D'Mello, J. Ellegood, V. Jakkamsetti, P. Liu, M.B. Nebel, GibsonJM, E. Kelly, F. Meng, C.A. Cano, J.M. Pascual, S.H. Mostofsky, J.P. Lerch, P. T. Tsai, Altered cerebellar connectivity in autism and cerebellar-mediated rescue of autism-related behaviours in mice, Nat. Neurosci. 20 (12) (2017) 1744–1751, https://doi.org/10.1038/s41593-017-0004-1.

[35] L. Mapelli, T. Soda, E. D'Angelo, F. Prestori, The Cerebellar Involvement in Autism Spectrum Disorders: From the Social Brain to Mouse Models, Int J. Mol. Sci. 23 (7) (2022 Mar 31) 3894, https://doi.org/10.3390/ijms23073894.

[36] L.M. Sydnor, K.A. Aldinger, Structure, function, and genetics of the cerebellum in autism, J. Psychiatr. Brain Sci. 7 (2022) e220008, https://doi.org/10.20900/jpbs.20220008.

[37] M. Greter, I. Lelios, A.L. Croxford, Microglia Versus Myeloid Cell Nomenclature during Brain Inflammation, Front Immunol. 6 (2015 May 26) 249, https://doi.org/10.3389/fimmu.2015.00249.

[38] J.D. Cherry, J.A. Olschowka, M.K. O'Banion, Neuroinflammation and M2 microglia: the good, the bad, and the inflamed, J. Neuroinflamm. 11 (2014 Jun 3) 98, https://doi.org/10.1186/1742-2094-11-98.

[39] S. Yona, K.W. Kim, Y. Wolf, A. Mildner, D. Varol, M. Breker, D. Strauss-Ayali, S. Viukov, M. Guilliams, A. Misharin, D.A. Hume, H. Perlman, B. Malissen, E. Zelzer, S. Jung, Fate mapping reveals origins and dynamics of monocytes and tissue macrophages under homeostasis, Immunity 38 (1) (2013 Jan 24) 79–91, https://doi.org/10.1016/j.immuni.2012.12.001. Epub 2012 Dec 27. Erratum in: Immunity. 2013 May 23;38(5):1073-9.

[40] R.C. Paolicelli, G. Bolasco, F. Pagani, L. Maggi, M. Scianni, P. Panzanelli, M. Giustetto, T.A. Ferreira, E. Guiducci, L. Dumas, D. Ragozzino, C.T. Gross, Synaptic pruning by microglia is necessary for normal brain development, Science 333 (6048) (2011 Sep 9) 1456–1458, https://doi.org/10.1126/science.1202529.

[41] E.C. Cope, B.A. Briones, A.T. Brockett, S. Martinez, P.A. Vigneron, M. Opendak, S. S. Wang, E. Gould, Immature Neurons and Radial Glia, But Not Astrocytes or Microglia, Are Altered in Adult Cntnap2 and Shank3 Mice, Models of Autism, ENEURO.0196-16.2016, eNeuro 3 (5) (2016 Oct 17), https://doi.org/10.1523/ENEURO.0196-16.2016.

[42] L.T. Nguyen, P.M. Nguyen, H.P. Nguyen, H.T. Bui, L.T.M. Dao, et al., Outcomes of autologous bone marrow mononuclear cell administration combined with educational intervention in the treatment of autism spectrum disorder: a randomized, open-label, controlled phase II clinical trial, Stem Cell Res Ther. 16 (1) (2025 May 30) 268, https://doi.org/10.1186/s13287-025-04404-4.

[43] E. Soliman, E.K. Gudenschwager Basso, J. Ju, A. Willison, M.H. Theus, Skull bone marrow-derived immune cells infiltrate the injured cerebral cortex and exhibit anti-inflammatory properties, Brain Behav. Immun. 123 (2025 Jan) 244–253, https://doi.org/10.1016/j.bbi.2024.09.023.

[44] D.E. Akinyemi, R. Chevre, O. Soehnlein, Neuro-immune crosstalk in hematopoiesis, inflammation, and repair, Trends Immunol. 45 (8) (2024 Aug) 597–608, https://doi.org/10.1016/j.it.2024.06.005.
[45] M. Sztretye, B. Dienes, M. Gönczi, T. Czirják, L. Csernoch, L. Dux, P. Szentesi, A. Keller-Pintér, Astaxanthin: A Potential Mitochondrial-Targeted Antioxidant Treatment in Diseases and with Aging, Oxid. Med Cell Longev. 2019 (2019 Nov 11) 3849692, https://doi.org/10.1155/2019/3849692.
[46] K.J. Tracey, Reflex control of immunity, Nat. Rev. Immunol. 9 (6) (2009 Jun) 418–428, https://doi.org/10.1038/nri2566.
[47] Y. Wei, T. Wang, L. Liao, X. Fan, L. Chang, K. Hashimoto, Brain-spleen axis in health and diseases: A review and future perspective, Brain Res Bull. 182 (2022 May) 130–140, https://doi.org/10.1016/j.brainresbull.2022.02.008.
[48] R.R. Ambati, S.M. Phang, S. Ravi, R.G. Aswathanarayana, Astaxanthin: sources, extraction, stability, biological activities and its commercial applications–a review, Mar. Drugs 12 (1) (2014 Jan 7) 128–152, https://doi.org/10.3390/md12010128.
[49] L. Zhao, X. Tao, K. Wang, Y. Song, B. Zhang, L. Yang, Z. Wang, Astaxanthin alleviates fibromyalgia pain and depression via NLRP3 inflammasome inhibition, Biomed. Pharm. 176 (2024 Jul) 116856, https://doi.org/10.1016/j.biopha.2024.116856.
[50] S.S. Moy, J.J. Nadler, A. Perez, R.P. Barbaro, J.M. Johns, T.R. Magnuson, J. Piven, J.N. Crawley, Sociability and preference for social novelty in five inbred strains: an approach to assess autistic-like behaviour in mice, Genes Brain Behav. 3 (5) (2004) 287–302, https://doi.org/10.1111/j.1601-1848.2004.00076.x.
[51] J. Caston, N. Jones, T. Stelz, Role of preoperative and postoperative sensorimotor training on restoration of the equilibrium behaviour in adult mice following cerebellectomy, Neurobiol. Learn Mem. 64 (3) (1995) 195–202, https://doi.org/10.1006/nlme.1995.0002.
[52] O. Friard, M. Gamba, BORIS: a free, versatile open-source event-logging software for video/audio coding and live observations, Methods Ecol. Evol. 7 (2016) 1325–1330, https://doi.org/10.1111/2041-210X.12584.